2017-01-01

Methods For Producing Graphene From Petroleum By-Products

Eva M. Deemer
University of Texas at El Paso, emdeemer@utep.edu

METHODS FOR PRODUCING GRAPHENE FROM PETROLEUM BY-PRODUCTS

EVA MARIE DEEMER

Doctoral Program in Materials Science and Engineering

APPROVED:

Russell R. Chianelli, Ph.D., Chair

Deidra R. Hodges, Ph.D.

Anupama Kaul, Ph.D.

Felicia S. Manciu, Ph.D.

Charles Ambler, Ph.D.
Dean of the Graduate School

Dedication

To my parents who personify the meaning of dedication.
Love you.

METHODS FOR PRODUCING GRAPHENE FROM PETROLEUM BY-PRODUCTS

by

EVA MARIE DEEMER, B.S. Chemistry

DISSERTATION

Presented to the Faculty of the Graduate School of

The University of Texas at El Paso

in Partial Fulfillment

of the Requirements

for the Degree of

DOCTOR OF PHILOSPHY

Department of Materials Science and Engineering

THE UNIVERSITY OF TEXAS AT EL PASO

May 2017

Acknowledgements

Thanks to all who encouraged me to continue the work, it was worth it. Thanks to Harry Chou who helped me with single layer graphene growth at UT Austin and contributed immensely to the fourth chapter of this thesis. Russ, you allowed me total freedom and supported me in pursuing my potential - you will never be replaceable.

Table of Contents

List of Tables

List of Figures

List of Illustrations

.

Chapter 1: Carbon Molecular Electronics

All electronic processes in nature occur using carbon-based molecular structures; from signal transduction in the brain all the way to photosynthesis in a leaf. Carbon Molecular Electronics (CMEs) as a field has been the result of recent developments in the interdisciplinary field with increasing numbers of synthetic and quantum chemists, physicists and engineers. New analytical tools and device architectures have been designed and investigated for the exciting realization of CMEs for photovoltaics, transistors, switches and other non-linear electronic components [1].

1.1. Need for CMEs:

Electronic devices such as radios, the telephones and wartime developments such as radar have been driven by the expansion of communication. These devices used crystals with semi-conductive properties to provide signal amplification and to convert alternating current (AC) to direct current (DC). Although the distances across which these communications could be carried advanced rapidly, they were subject to frequent burn outs.

In 1915, AT&T was the first company to successfully utilize transcontinental communications system using vacuum tubes. After World War II, the technological focus was on using solid state devices to improve these electronics. In 1945, AT&T founded Bell Labs to enable solid state physics researchers to work on amplifying devices. By 1947, Bell Labs created the first transistor using a point contact device on a Germanium slab. The design was improved a year later in 1948 with the advent of the bipolar junction. In 1954 Germanium was replaced by a cheaper element Silicon making it feasible for researchers at Texas Instruments develop the Integrated Circuit by 1958 [2]. The computational power of the late 50's was stimulated by this integration of complete circuitry (wires, transistors, resistors and capacitors and by 1961 the junction transistor was replaced with field effect transistor (FET). This device made the semi-conducting "on-off"

switching mechanism faster by applying a voltage bias across a conducting channel to limit the flow of electrons, thereby manipulating an on/off state without having to actually apply or limit voltage to the switch itself.

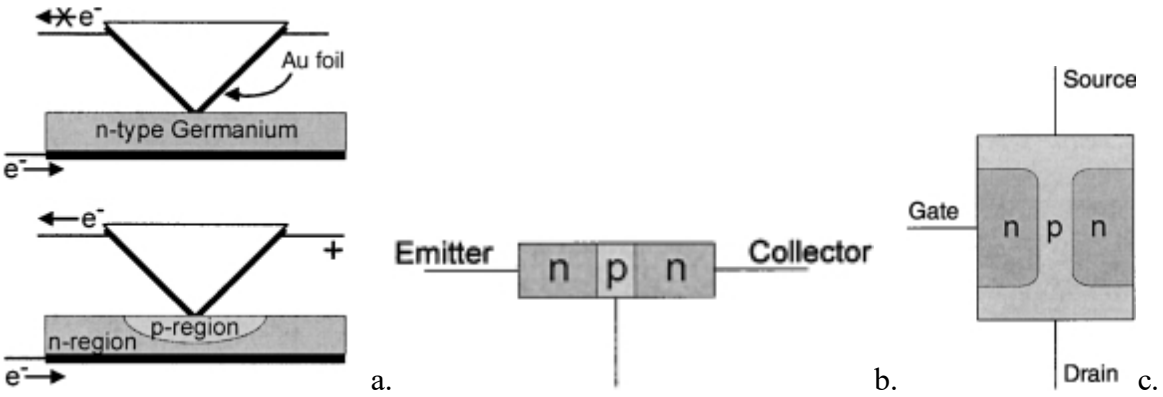

Illustration 1.1: Evolution of the transistor device (a.) transistor (b.) the biopolar junction (c.) the field effect transistor [3].

By 1965, Intel Co-founder Gordon Moore, made a prediction that the number of transistors per cm^2 on devices would double every year for the next 10 years [4]. Today the statement known as "Moores law" is well accepted and refers to the predicted trend that computational power per unit area doubles every 18 months [5]. Progress in communication and computational devices was paralleled by an unprecedented advancement in society and an estimated $3 trillion (USD) of additional value has been added to the gross world product (GWP), plus another $9 trillion (USD) of indirect value in the last 20 years, which can be correlated to the pace of innovation projected by Moore's Law (Illustration 1.2) [6]. This is worth more than the gross domestic products (GDP) of France, Germany, Italy and the United Kingdom combined.

Advances have been made across all industries as a result of this digital processing power. Computation has aided the development of new materials, bio-fuels and feedstock's for plant-based chemicals. One petaflop is roughly equal to one quadrillion calculations per second and today's super computers are capable of using petaflops to solve some of the world's biggest problems.

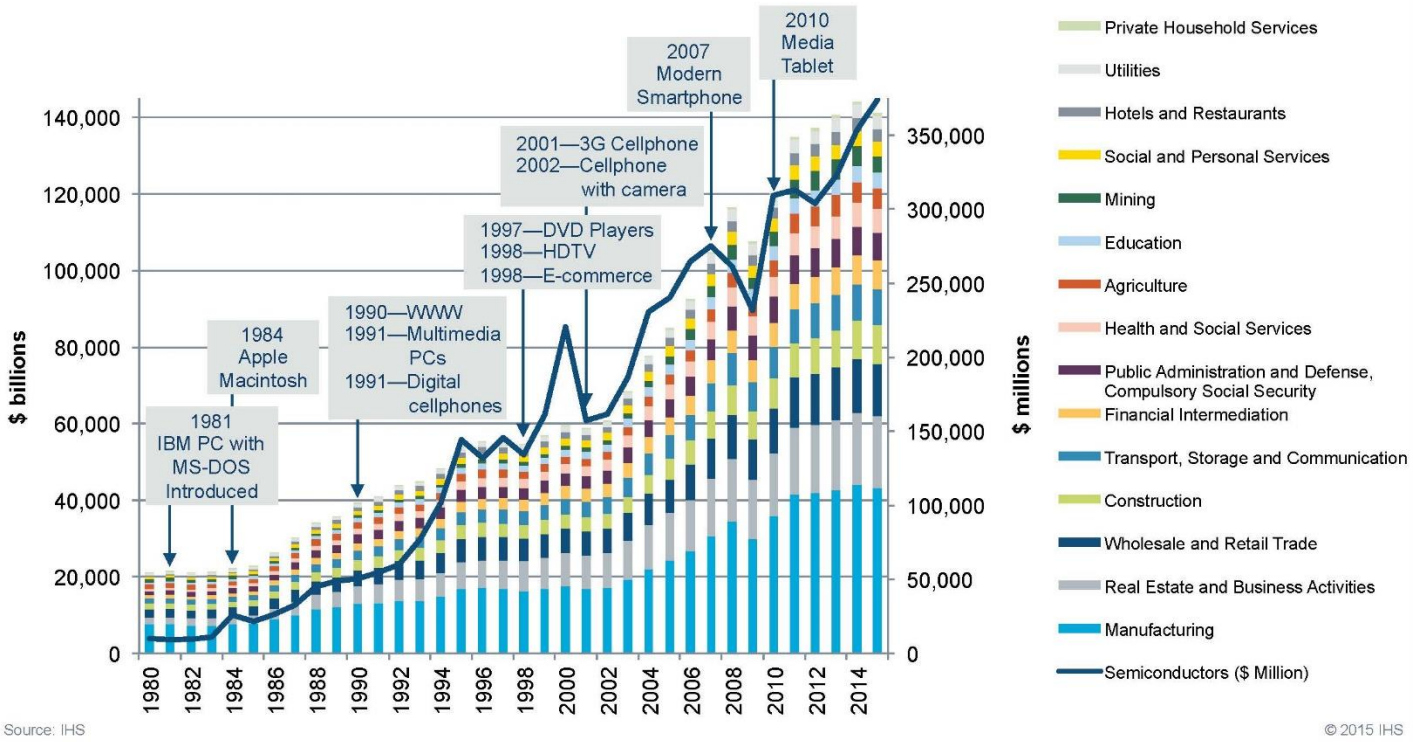

Illustration 1.2: Semiconductor growth plotted with worldwide gross output by industry in USD Billions (left axis) and semiconductor sales in USD Millions (right axis) [6].

We are now entering the final limit for these devices as their performance is increasingly compromised by their own intrinsic properties as their size decreases. Instead of current travelling along system components, there is more tendency for current to tunnel in between components instead. The industry looking for ways to innovate devices by increasing current density but reducing bulk weight.

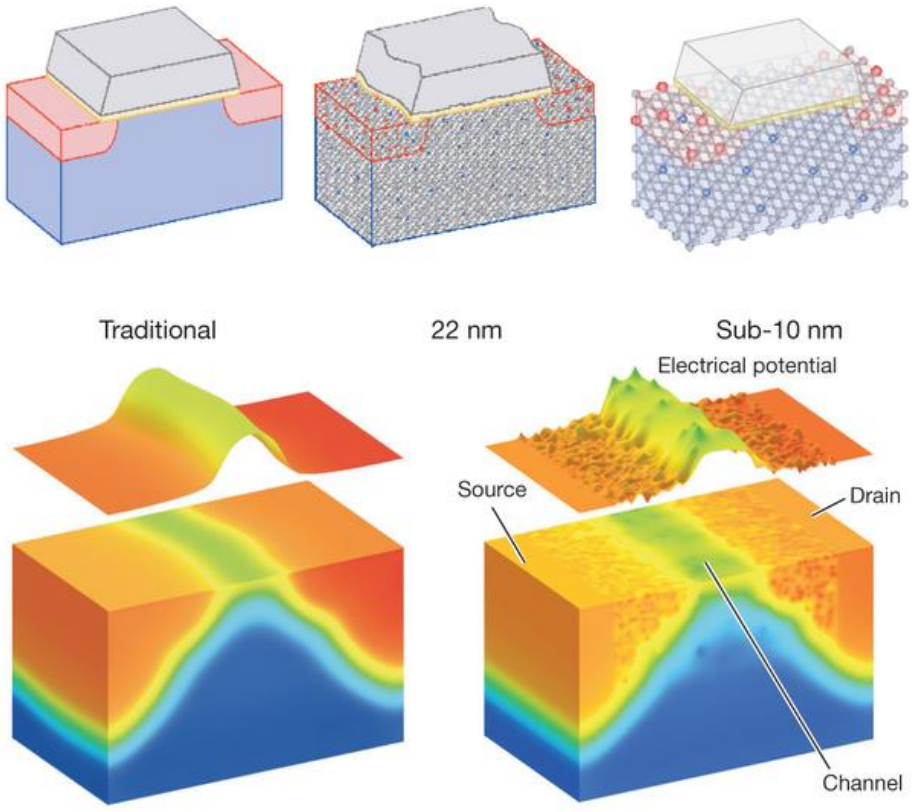

Illustration 1.3: As a metal oxide–semiconductor field effect transistor (MOSFET) shrinks, the gate dielectric (yellow) thickness approaches several atoms (0.5 nm at the 22-nm technology node) (top) [7]. Atomic-level manufacturing variations, especially for dopant atoms, start affecting device parameters, making each transistor slightly different (bottom) [8].

In 1959, Richard Feynman suggested this vision:

> "*I don't know how to do this on a small scale in a practical way, but I do know that computing machines are very large; they fill rooms. Why can't we make them very small, make them of little wires, little elements–and by little, I mean little. For instance, the wires should be 10 or 100 atoms in diameter, and the circuits should be a few thousand angstroms across...there is plenty of room to make them smaller. There is nothing that I can see in the physical laws that says the computer elements cannot be made enormously smaller than they are now. In fact, there may be certain advantages*." [9]

State-of-the-art commercial microcomputer chips today contain more than 10-50 million switches in an area the size of a large postage stamp. A future device will have molecules for circuitry and be about a million times denser that today's devices. In addition to this change in the density of computation, molecules are likely to change the nature and applications of computation. Electrons in molecules are limited to quantum energy levels within molecular structures and using them as devices will make computation a literal property of matter. Building prototype molecular-scale electronic computing systems will produce a quantum jump in computation, and revolutionize electronic computation, molecular modeling and materials science [10].

Table 1.1: Current density of molecular wires expressed in nanoscale units compared to current density of macroscopic copper [11].

Device	Area cross sectional (nm^2)	Current Density (electrons/nm^2-sec)
1 mm copper wire	3×10^{12}	2×10^{6}
Polyphenylene wire	0.05	4×10^{12}
Carbon nanotube	3	2×10^{11}

Experiments done in the mid and late 1990s demonstrated individual molecules can possess physical phenomena which previously thought to have been limited to semiconductors and revolutionized the material science. In 1996, it was still questionable whether or not individual molecules could actually conduct electricity but experiments performed from 1995 to 1997 [12-17] determined that individual molecules can conduct and also switch small electrical currents [18-23]. These pioneering works demonstrated the use and assembly of molecular scale devices using aromatic organic molecules, nanotubes, biomolecules or nanowires (Table 1.1.).

1.1.1. Organic Based Molecular Electronic

The organic photovoltaic (OPV) cell [24], organic field-effect transistor (OFET) [25], and organic light emitting diode (OLED) [26] were demonstrated in the mid-1980s and generated interest for organic electronic devices throughout academic and industrial institutions. The discovery that molecules can be electronic components would make all-plastic integrated circuits, where each pixel consists of an OLED driven by an OFET [27] into a real possibility.

Controlling the molecular organization of these devices relies on using chemical design and physical processing to facilitate long-range ordering [28] on the surface of a substrate. Conjugated molecules have been explored for use in organic electronics and vary widely, however conjugated discotic materials and their self-assembly have also been of interest due to their unique liquid crystalline properties [29, 30].

Molecules forming discotic mesophases are typically made of a central rigid discotic conjugated core substituted by flexible substituents and their liquid crystallinity originates from the microphase segregation of these two constituents. These molecules have crystalline character promoted by the interaction between the conjugated cores and a liquid character from the melting of saturated alkyl chains in the mesophase [31]. Discotic molecules can organize spontaneously into columnar superstructures that are one-dimensional, which possess self-healing properties (i.e., the capability of repairing structural defects upon thermal annealing in contrast to crystalline materials). They can also be oriented by external fields. The aromatic constituents in the columnar superstructure serve as a media for one-dimensional electron transport.

In recent years, discotic system with expanded aromatic cores has been the subject of many research efforts [32]. It has been noted that larger aromatic cores can enhance higher supramolecular order, columnar stability in discotic liquid crystals and improve charge-transport property due to a more extended π-orbital overlap. Polycyclic aromatic hydrocarbons (PAHs), belonging to the family of discotics with an average diameter smaller than 10 nm (also called nano-

graphenes), can be regarded as two-dimensional graphene segments composed entirely of sp^2 carbons. These graphene-type molecules hold advantages over other graphene materials (graphene sheet and graphene nanoribbon) in terms of structural perfection, production scale and physical process-ability. Synthesizing these extended PAHs involves intramolecular cyclodehydrogenation and planarization of hyperbranched polyphenylene precursors [33].

1.1.2. Nano-carbon based electronics

Carbon occurs naturally in many forms as a component in countless substances and is one of the most common atoms on Earth. Despite those facts, only a two materials contain nothing but carbon: the carbon allotropes diamond and graphite. Graphite is composed of layers with sp^2 bonded carbon atoms in a honeycomb arrangement and is the most common form of pure carbon. Layers are held together weakly by Van der Waals forces which produces a small valence and conduction band overlap of about 40 meV making graphite overall a *semi-metal*. The electronic structure of graphene, an individual layer of graphite, was first discussed by P. R. Wallace in 1947 in the context of graphite [34].

Buckyballs, carbon nanotubes, and graphene are carbon nanostructures widely researched today for their electronic properties and represent a class of nano-scale carbon allotropes. A buckyball is created by collapsing a dimension of graphite into a hollow "soccer ball –like" sphere of 60 carbon atoms. First discovered in 1985, it was a Nobel Prize winning material within a decade and was the first carbon nanomaterial to gain widespread attention. Buckyballs have many proposed uses, such as encapsulation of reactive compounds in chemistry, isolation of quantum systems for functional quantum bits, and in fundamental quantum experiments it is the largest one of the largest materials that can act as both a particle and a wave.

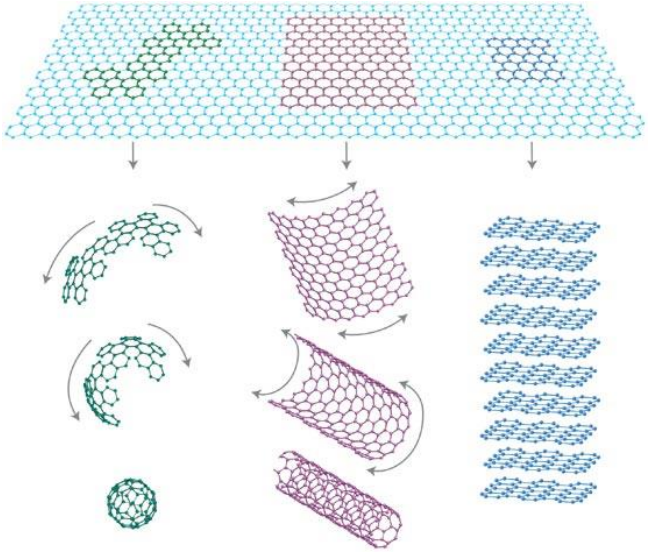

Illustration 1.4: Graphite and its related nanocarbons; the buckyball, the carbon nanotube and graphene [35].

1.1.2.1. Carbon Nanotubes (CNTs)

Carbon nanotubes (CNTs) can be thought of as strip of graphene that have been rolled into a tube. While they are only nanometers in diameter, CNTs can grow to millimeters in length and because of the strength of the bonds in a hexagonal carbon lattice, nanotubes are one of the strongest fibers ever discovered. Additionally, CNTs can display both metallic and semiconducting electric properties due to the extra quantum confinement imposed on electrons along the circumferential axis. CNTs can function as wires, transistors, and nonvolatile memory elements, suggesting the possibility of nanometer scale integrated circuit design. Research groups have also shown that crossed nanotubes can be welded together with exposure to an electron beam in the presence of carbon impurities, thus allowing for separate nanotubes to be linked together [36]. Nanotubes have also been demonstrated as transistors which operate very similarly to conventional FETs. Researchers are also able to produce doped n-type and p-type regions using conventional methods [37].

1.1.2.2. Graphene

While graphite has been used for ages in a range of applications from lubricant to pencils, researchers only been studying graphene since1990. For the first decade, research was hindered due to the difficulty of producing two dimensional graphene in electrically isolated environments and without defects. In 2004, two researchers named Andre Geim and Konstantin Novoselov at Manchester University produced high quality graphene easily through mechanical exfoliation with scotch tape [38]. This breakthrough gave researchers access to pure graphene easily in a number of environments desirable for experimentation. Furthermore, they found that if silicon with a 300 nanometer oxide layer was used as a substrate for the single layer graphene flakes, they could be seen as a discoloration under any optical microscope. These properties made it possible to perform electrical and nano-mechanical experiments on graphene that began to validate the material's novel properties. The scotch tape method sparked widespread research on graphene in many areas of physics and materials science, and quickly won Geim and Novoselov the Nobel Prize in Physics in 2010.

In most conductors, the valence and conduction bands overlap, giving excited electrons many states to occupy as they move throughout the material. This property is known almost exclusively in a class of materials or atoms known as metals. While graphene is an excellent conductor it is a zero-bandgap semiconductor and it is not a metal. While the valence and conduction bands do not overlap in graphene, they touch at the Fermi level [39].

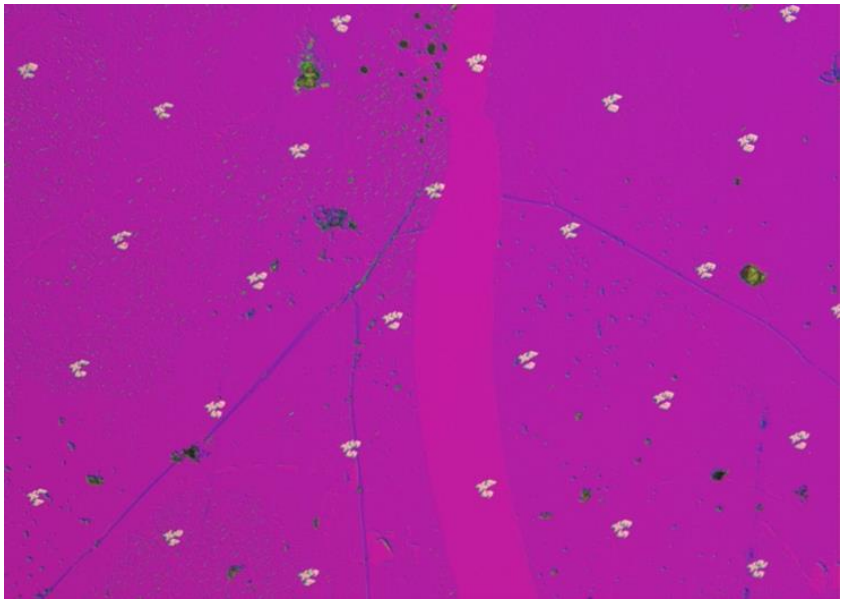

Figure 1.1. Single Layer Graphene (SLG) grown at UT Austin transferred to Si wafer with 300 nm oxide layer showing discoloration of SLG

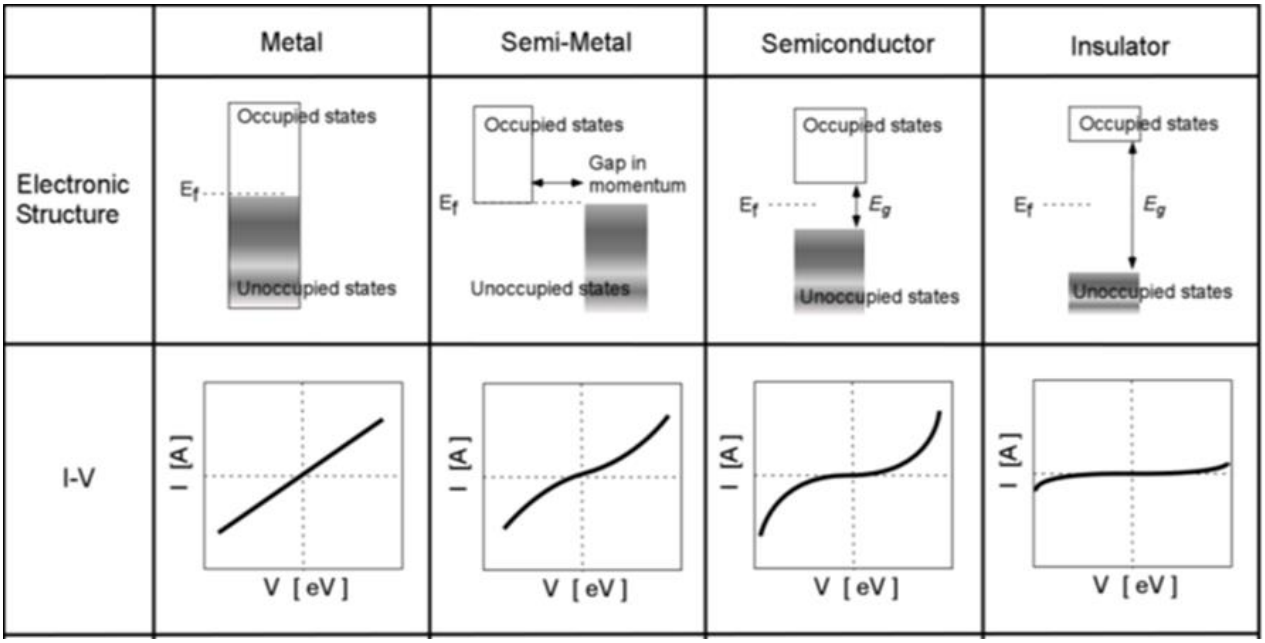

Illustration 1.5. Material electronic structures and corresponding I (V) Curves [40]

1.1.3. Asphaltene

Asphaltenes are very unfamiliar class of hydrocarbon component in crude oils [41]. Naturally occurring hydrocarbon fluids from crude oil are compounds that span a continuum of composition from dry natural gas to tar. Across that range, density and viscosity increase dramatically and color changes from clear to deep brown as asphaltene content increases from 0 to nearly 20%. Certain properties of asphaltenes have been known since before the first commercial oil wells were drilled [42]. In 1837, J.B. Boussingault defined asphaltenes as the residue from the distillation of bitumen: insoluble in alcohol but soluble in turpentine [43]. The definition used today is related: insoluble in n-alkanes but soluble in toluene. Asphaltenes obtained in this way are dark colored solids with a density of about 1.2 g/cm^3. They are also infusible, meaning they have no defined melting point, but they do decompose when heated, leaving a carbonaceous residue. As far as asphaltene structure is concerned, researchers agree that some of the carbon and hydrogen atoms are bound in ring-like, aromatic groups, which also contain the heteroatoms. Alkane chains and cyclic alkanes contain the rest of the carbon and hydrogen atoms and are linked to the ring groups. Within this framework, asphaltenes exhibit a range of molecular weight and composition. This compositional characterization is accepted by nearly all asphaltene specialists, but leaves ample room for debate about the structure or size of individual asphaltene molecules.

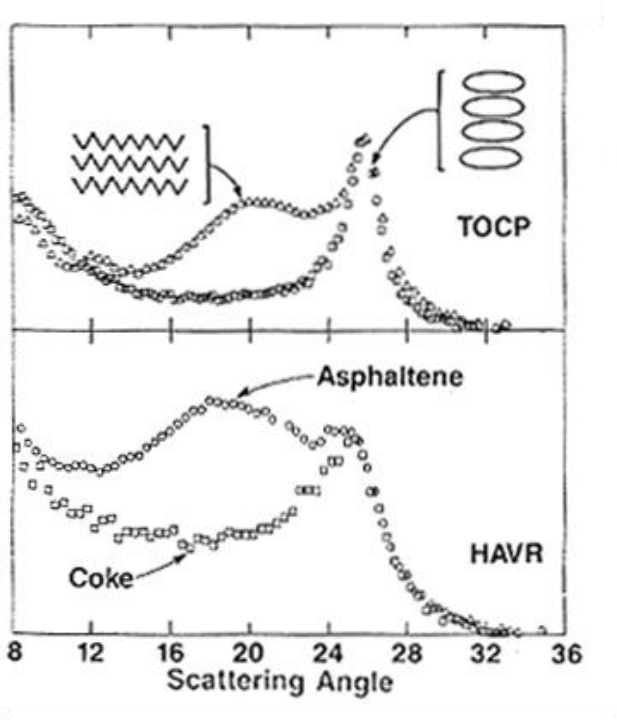

Illustration 1.6. X-Ray Diffraction of Asphaltene –High Aromatic Vacuum Residue (HAVR) compared to synthetic molecule (TOPC) [44].

Asphaltene structure has been extensively studied by Chianelli et. al and found to have a structure similar to that of the synthetic compound tetraoctyl carboxylate perylene (TOPC) [44]. X-Ray diffraction (XRD) studies performed on TOPC (shown in Illustration 1.6) differentiate two peaks that can determine distinction between alkane chains and stacked aromatic cores. Using these synthetic structures as a model, researchers were able to define the structure of asphaltene before and after exposure to heat using XRD and the results show that the production of coke is actually the self-assembly of stacked aromatic cores.

Chapter 2: SCANNING PROBE MICROSCOPY

Scanning probe microscopy (SPM) was developed in the 1980s to enable scientists to investigate surfaces with atomic resolution. We can no longer "see" at distances of 275 nanometers with visible light. After the invention of SPM, scientists could not only "see" atoms but also manipulate them and study their properties which represented an extraordinary breakthrough in the field of nanotechnology.

2.1. Background

In the early 1980's, Gerd Binnig and Heinrich Rohrer began investigating the possibility of using electron tunneling to probe the surface of conductors and semiconductors [45-47]. In 1983, they succeeded in producing an image with atomic resolution of the surface of Silicon (111). It was this image that caught the attention of the surface science world and resulted in a Nobel Prize in 1986. The discovery led to the scanning tunneling microscopy (STM); the first microscopic tool to observe atoms in real space. In addition to the atomic resolution, tunnel currents could also be studied providing insight into the local density of state (LDOS) which represent electron densities (orbitals) of atoms in materials. A brief timeline lists these events is below:

- 1981: Dr. Binnig and Dr. Rohrer invent the scanning tunneling microscope (STM).
- 1982: Dr. Binnig and Dr. Rohrer are the first people to "see" atoms when they use an STM to create an image of a silicon sample.
- 1985: Dr. Binnig, Dr. Christoph Gerber (IBM Zurich Research Center), and Dr. C. F. Quate (Stanford University) develop the atomic force microscope (AFM).

- 1986: Dr. Binnig and Dr. Rohrer are awarded the Nobel Prize in physics for the invention of the STM.
- 1987: Tom Albrecht of Stanford University is the first person to use an AFM to create images of individual atoms.
- 1988: AFM becomes available commercially.

2.1.1. Scanning Tunneling Microscopy

The particle-wave dualism refers to the description of electrons as both a particle and a wave. With the wave character of matter, particles exhibit a probability of existence at places where classically they should not exist. One of these phenomena is the tunnel effect, which describes the ability of an electron to tunnel through a vacuum barrier from one electrode to the other.

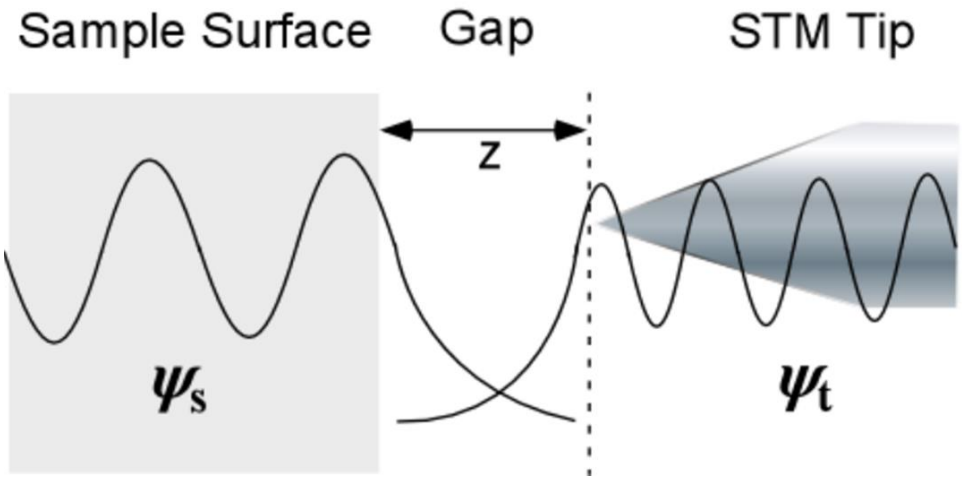

Illustration 2.1: Illustration of the operating principle of STM: the overlap in wave functions at the atomic level at a distance of z [40]

In STM bias voltage is applied between an atomically sharp conductive tip and a conductive sample, so when the sample is approached to a few angstroms from the tip, tunneling current occurs, that indicates proximity of the tip to the sample with very high accuracy.

2.1.1.1. Constant Current

In Constant Current mode (CCM) of operation the scanner keeps the current constant by using a feedback circuit when scanning sample surface. Any vertical displacement of the scanner (feedback signal) is a reflection of the surface topography. STM can give true atomic resolution on some samples at ambient conditions but can only be applied to conductive samples or thin nonconductive films on conductive substrates [48]. The speed of scanning in CCM is restricted by the feedback system. The tunnel currents recorded during the measurement are from 0.03 nA all the way down to 0.01 nA, so it is possible to investigate low conductivity surfaces, such as biological objects. STM images are determined by the surface topography, the density of states, bias voltage, and current value [48].

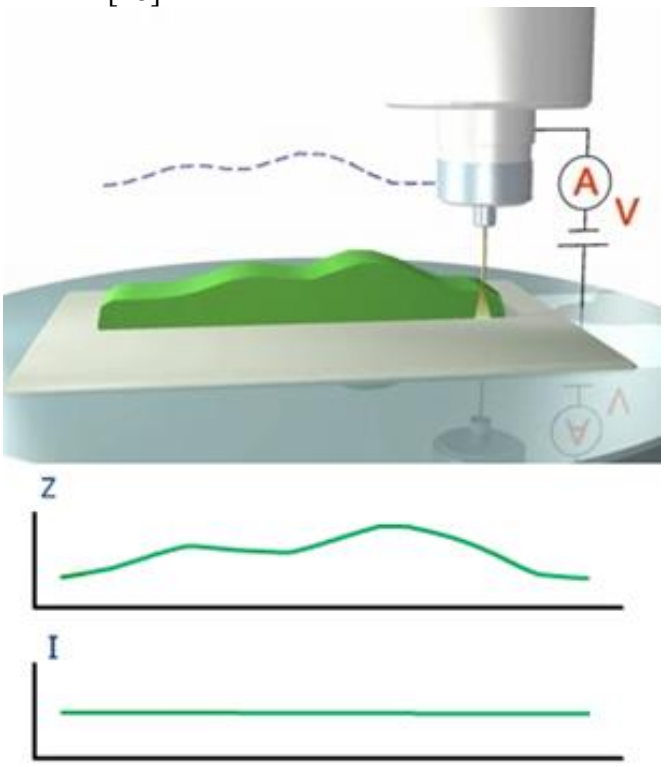

Illustration 2.2: Constant Current Mode where z is height and I is current [49]

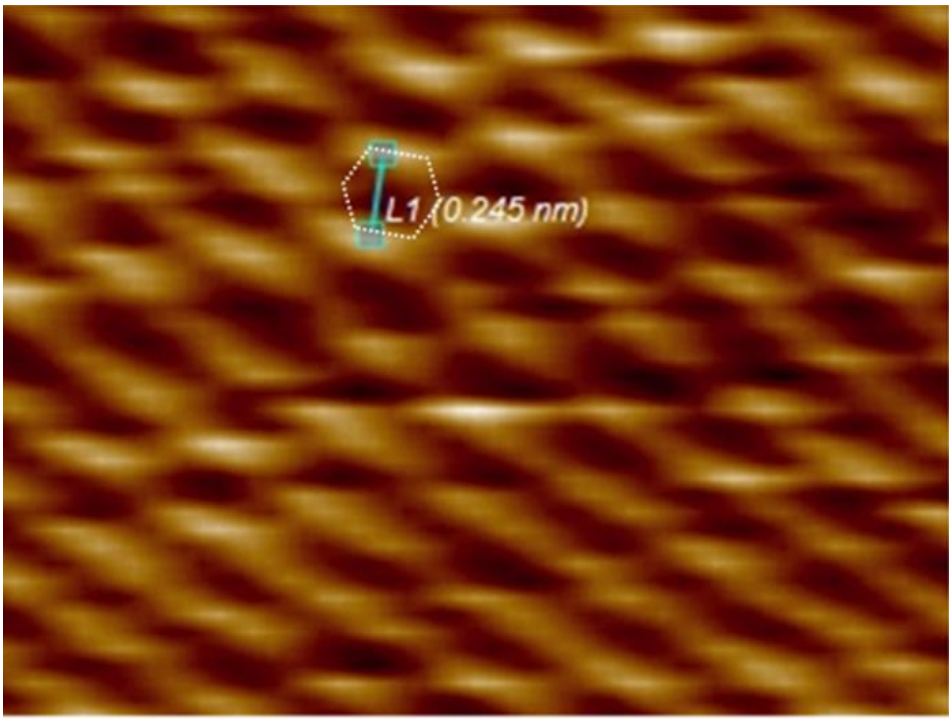

Figure 2.1. Highly ordered pyrolytic graphite in constant current mode showing the lattice vector of ~2.45 angstroms taken at UTEP (0.05 nA Bias and 0.101 nA current)

2.1.1.2. Constant Height

In Constant Height mode (CHM) the STM scanner operates the tip only in one plane, so that current between the tip and the sample surface visualizes the samples discontinuity. This mode does not adjust for the sample height so a higher scan speed can be used. However, this means that CHM should only be applied to a very flat surface as any surface roughness greater than 5-10 Å will cause the tip to crash. The weak feedback is still required to maintain a constant average tip-sample distance.

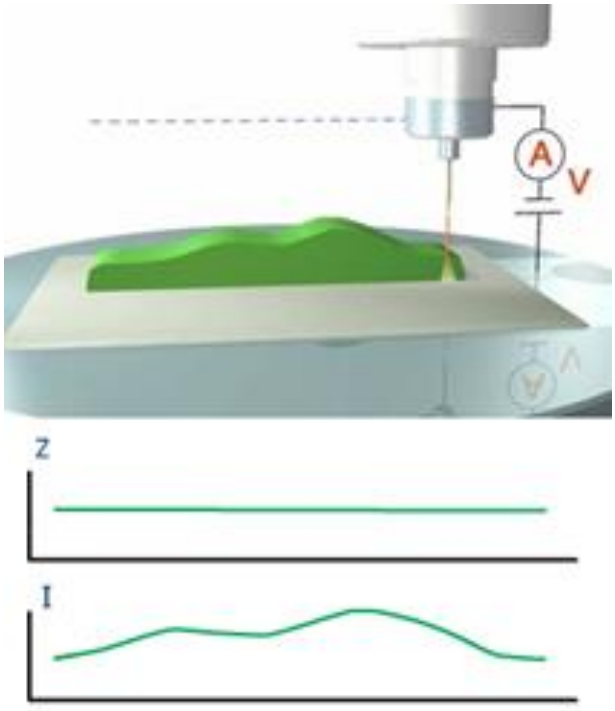

Illustration 2.3. Constant height mode where z is height and I is current [50].

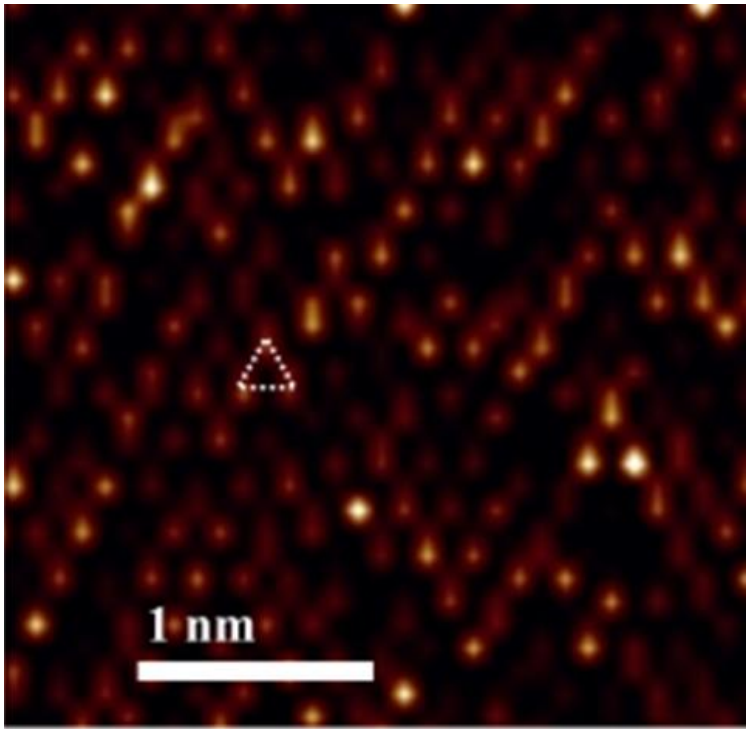

Figure 2.2. Highly ordered pyrolytic graphite in Constant Height Mode taken at UTEP (0.05 Bias and 0.101 nA current) showing A atoms within the stacked graphite plane.

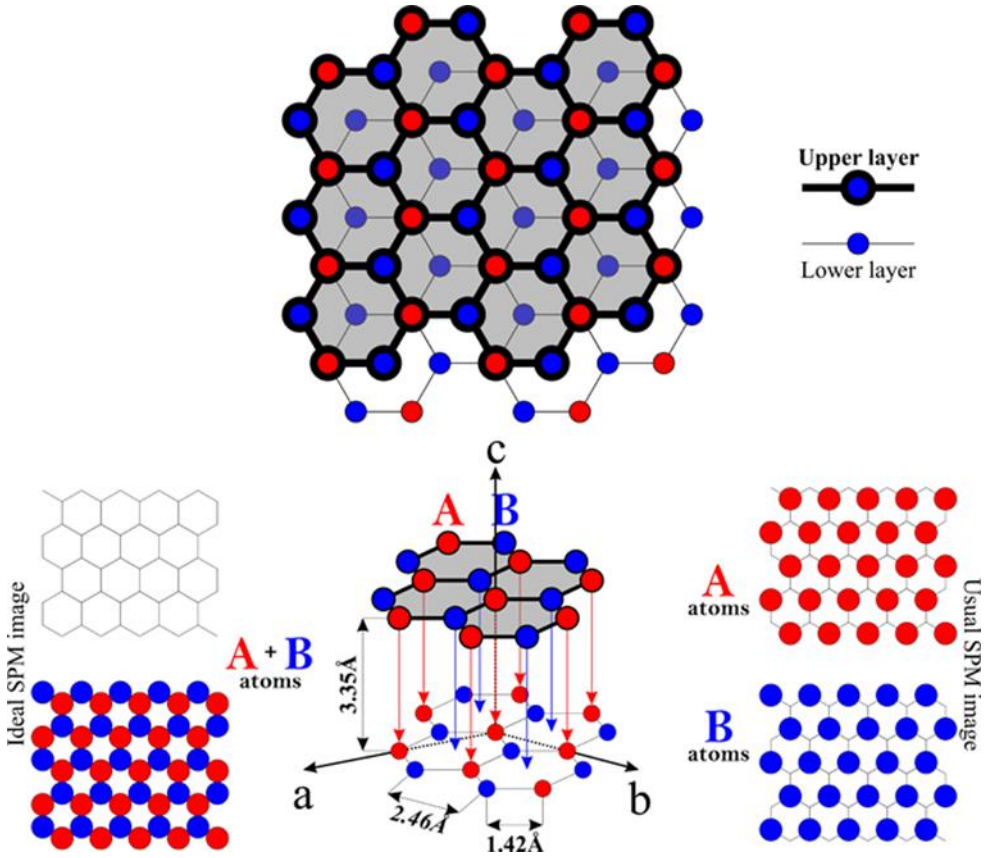

Illustration 2.4. Highly ordered pyrolytic graphite illustrated to show the lattice vector of 2.56 angstroms, the interlayer distance of 3.35 angstroms and the unit cell between A B atoms of 1.42 angstroms [51]

2.1.1.3. Scanning Tunneling current-voltage Spectroscopy

During Scanning Tunneling Spectroscopy (STS) a topographic image is acquired at a fixed current (I_0) and Voltage (V_0) and a series of points in the image feedback loop are interrupted and the bias voltage is set to a series of voltages (in these experiments +1 and -1) and the tunneling current (I) is recorded. The voltage is then returned to V_0 and the feedback loop is turned back on. Each current-voltage spectra can be acquired in a few milliseconds to minimize drift in the tip

position. This procedure generates a complete current image [I_i (x,y)] at each voltage [V_i] in addition to the topographic image [z (x,y)|V_0 I_0].

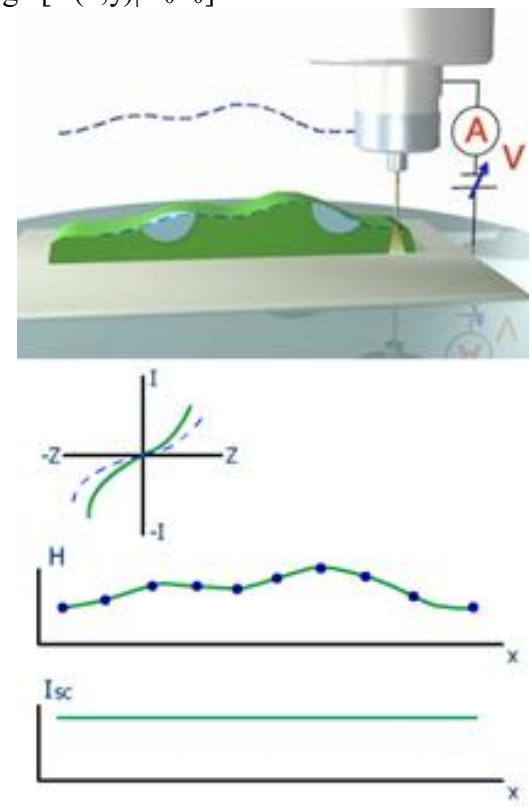

Illustration 2.5. Scanning Tunneling current-voltage Spectroscopy where H is height and I is scanning current [52].

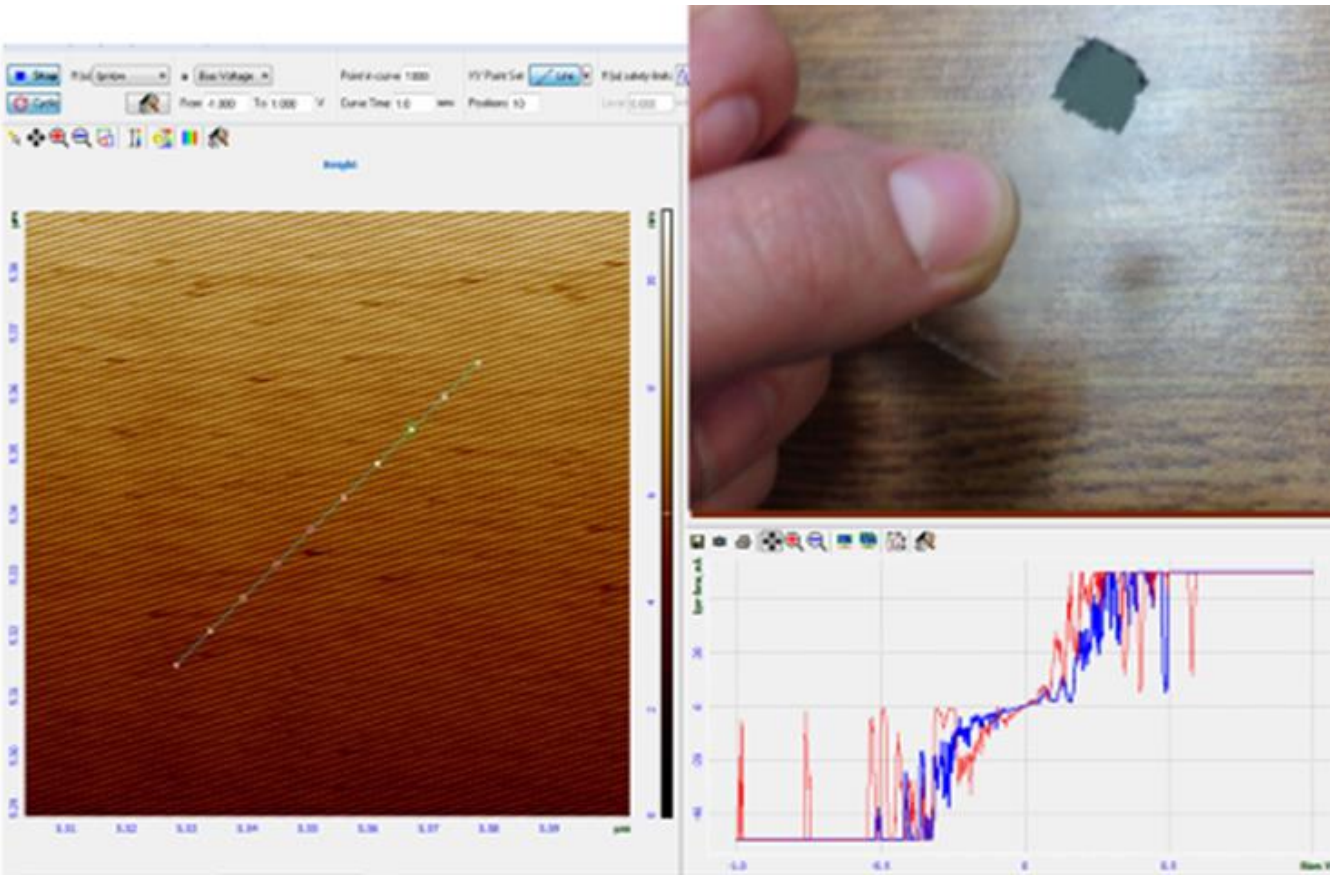

Figure 2.3. Cleaved HOPG surface (top right) for current-voltage measurements (bottom right) and Scanning Tunneling Spectroscopy experimental set-up cycling through ten points on the HOPG in constant current mode (left).

2.1.2. Atomic Force Microscope

The major disadvantage of the STM is that only conductive samples or conductive layers can be investigated. After developing the STM with success, Binnig guessed that a macroscopic cantilever provided with a nanometer sharp tip can be bent to a sufficiently large amount to be measured by the common capacities when interacting with sample surfaces through atomic forces [53].

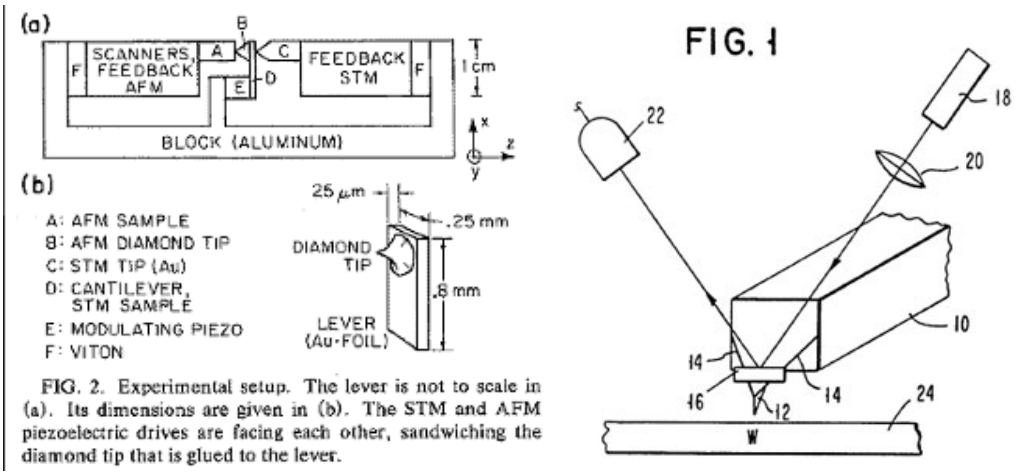

FIG. 2. Experimental setup. The lever is not to scale in (a). Its dimensions are given in (b). The STM and AFM piezoelectric drives are facing each other, sandwiching the diamond tip that is glued to the lever.

Illustration 2.6. The first AFM designed (left) [54] and the invention of the cantilever reflected laser [55].

As the tip scans a surface, inter-atomic forces between the tip and the sample surface induce displacement of the tip and corresponding bending of the cantilever. While bending was sufficient to measure this displacement, an improvement was made by adding a laser reflecting off the cantilever into a photodiode [55]. The output of this data is provided to a computer for processing and provides a topographical image of the surface with atomic resolution in 3-D.

Cantilevers are not just bent by direct contact but also interact with forces such as van der Waals, magnetic, electric and so on and because SPM can interact with these properties, there are a wide variety of SPM modes that can manipulate and analyze electromagnetic properties of materials at the atomic scale.

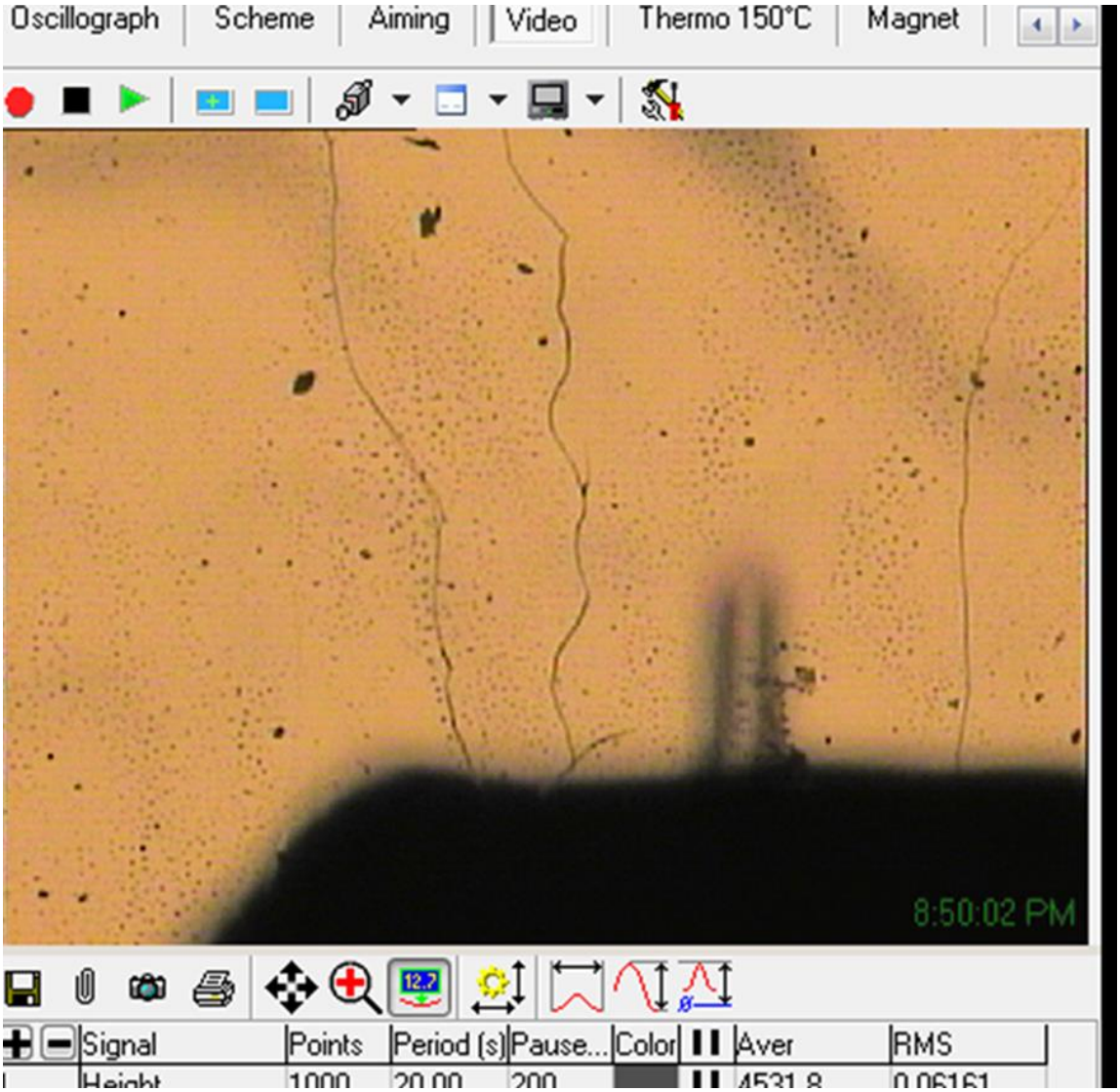

Figure 2.4. Optical Microscope Image of Atomic Force Microscope (AFM) experiments on HOPG with sample

Chapter 3. CONSEQUENCE OF OXIDATION METHOD ON LARGE AND SMALL GRAPHITE PRECIRSOR DURING SYNTHESIS OF GRAPHENE OXIDE

3.1. Introduction

Graphite oxide can be converted to single layer graphene oxide (GO) in polar solutions due to oxygen functional groups creating an electronegative repulsion. Consequently, it is desirable to improve the oxidation of graphite but without doing so at the expense of the carbon sp^2 hybridized structure. Graphene [56,57,58] is a promising material with extraordinary mechanical, electronic, magnetic and optical properties [59-67] that is anticipated to impact semiconductor and composite industries for a variety of applications in energy [68 -70]. However, differences between lateral and vertical dimensionalities of graphene define also differences in electronic performance for applications which impact the commercialization of graphene.

Graphite oxide is a widely used precursor for the bulk synthesis of GO which is then prepared into graphene either by a chemical or a thermal reduction route [71] due to the ease of preparation and low-cost. Chemical and thermal reduction can impart damage to the graphene basal planes and disrupt the carbon sp^2 hybridized structure depending on the reactivity of GO [72]. Zhao et al. previously studied the reduction of GO papers prepared via vacuum filtration using hydrazine, thermal annealing under Ar/H_2, and the combination of the two methods and found the latter to be most effective at restoring conductivity [73]. However, one of the disadvantages to hydrazine aside from its toxicity [74] is that it renders reduced GO insoluble [75] and difficult to apply to substrates. In addition, Su et al. found that during thermal annealing, ultra large GO sheets break into small domains [76]. Zhang et. al. measured the

conductivity of GO papers reduced using l-ascorbic acid (L-AA) and found them to be comparable to papers reduced by hydrazine. The results demonstrate an inexpensive and effective method for restoring conjugation without using high temperature thermal annealing [77] that is an environmentally friendly alternative without the need for surfactants to stabilize the resulting rGO dispersion.

Identifying and quantifying the various functional groups present in GO is complex task and to date there is still much debate about the structure of GO [78].Owing to the number of variables involved with synthesizing chemically derived graphene such as parent graphite, oxidation paths, chemical exfoliation methods and reduction methods, researchers have previously sought to understand the impacts on the resulting reduced GO devices. Various factors which would affect the size of GO sheets, such as post-treatment of parent graphite [79], oxidation conditions [80-82] pH value [83] and controlled centrifugation [84] have been explored. Chen et. al previously studied the impact parent graphites have on subsequent GOs with five different commercially sourced graphites using the Staudenmaier oxidation method [85]. They concluded that the properties of the parent graphite significantly influenced the properties of thermally reduced corresponding GO but did not explore further oxidation methods for comparison to the Staudenmaier oxidation method which produces GO that is relatively substochiometric. Qi et al. studied the effect GO flake size had on electrical resistance by preparing GO from a parent graphite of 200 μm and controlled flake size through various ultrasonication times [86]. Unavoidable fracturing of GO sheets during the oxidation and exfoliation processes results in GO sheets with smaller area than parent graphite and the consequently increasing inter-sheet contact resistance in conductive thin films due to a larger amount of inter-sheet junctions [87]. If the sp^2 conjugated carbon network is only partially

recovered, charge transport is less efficient through the atomically thin plane. As a result of all these reported properties, controlling the size of GO sheets essential for improving the performance of rGO devices. Synthesis of ultra large GO sheets was found to be controllable by modifying the oxidation/exfoliation [88, 89]. The results demonstrated higher degrees of oxidation and exfoliation after prolonged and more vigorous synthesis. However, researchers compared GOs after various reaction times or after increasing oxidant while consecutively sampling and the reaction took place using the same oxidation method (Hummers) throughout each of these experiments. Rodriguez-Pastor et. al. compared the structure of GO produced using the same parent graphite and found GO synthesized from Hummers method has significant amounts of oxidative debris compared to GO synthesized with Brodies method. The combination of $KMnO_4/H_2SO_4$ cuts the basal planes leaving formed edges with carbonyl groups [90] and results in either large-single sheets, or small (humic) and very small (fulvic) entities oxidized at the edges. However they determined this cutting mechanism optimizes the exfoliation into single sheets and found the combination of $KMnO_4/H_2SO_4$ to be more successful than $KClO_3$/ HNO_3 at producing single layers [91]. C. Shi et al. prepared GO from Marcano–Tour's improved method and Hummers method to determine how the procedures and reagents affected the structure of GO and rGO nanosheets produced after reduction with sodium borohydride [92]. They found that the addition of water during oxidation significantly influenced the resulting oxidation effects and the quality of GO produced from improved method was enhanced when ice was used instead of water in during oxidation. The study concluded that rGO prepared from Marcano–Tour's improved method was successful in producing rGO with less defects but this did not consider more than once size or source of parent graphite either.

Recently, Chowdhury et al. systematically studied the role of graphite precursor and $NaNO_3$ in GO produced from Hummers method utilizing various graphite sources and sizes (20, 40, 150μm) and found $NaNO_3$ reduced crystallite sizes of GO sheets due to higher oxidation in the basal plane [93]. The results suggested a potential way to use Hummers method and preserve the lateral dimensions of the parent graphite as GOs synthesized. In this work, we revisit Mercado-Tours study using Hummers method without $NaNO_3$ and with large and small commercial sources of graphite to investigate resulting GO and subsequent reactivity to L-AA.

Table 3.1. Summary of synthetic methods referenced and used in this work for comparison. Reagents added to 3 grams of graphite.

Method	Product	$NaNO_3$ (g)	H_2SO_4 (ml)	$KMnO_4$ (g)	H_3PO_4 (ml)	Reaction conditions
Hummers' method [99]	HGO	1.5	69	9	/	Reacted for > 1 hr at 35C, quenched in water
Hummers' method [99]	HGO+	1.5	69	18	/	Reacted for ~20 hrs at 35°C, quenched over ice
Improved method [99]	IGO	/	360	18	40	12 hrs at 50°C, quenched over ice
Hummers method [93]	HGO	/	69	9	/	Reacted for 2 hours at 35°C, quenched over ice

3.2. Experimental

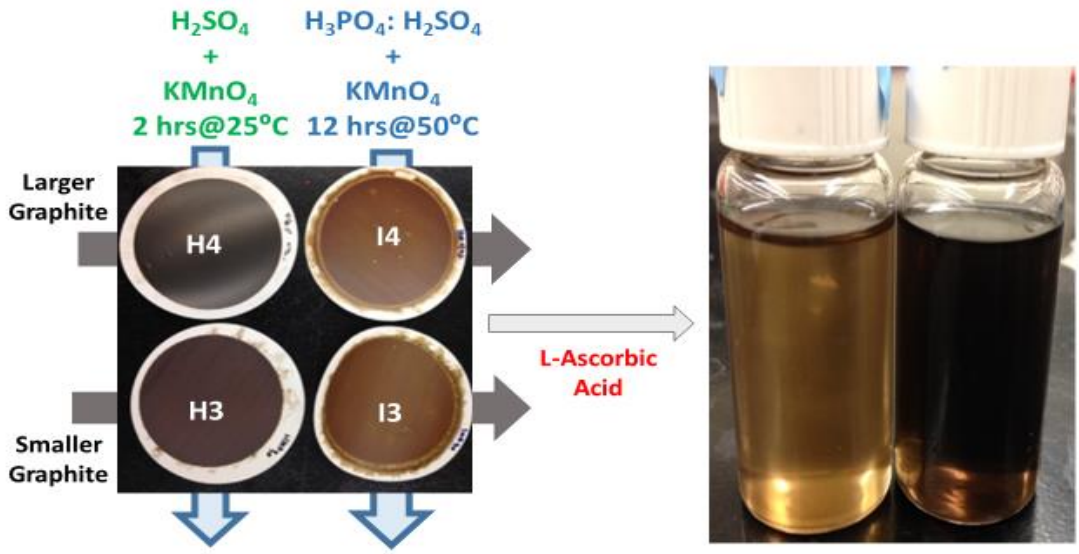

Illustration 3.1: Experimental overview of Graphene Oxide synthesis (left) and reduction (right).

3.2.1. Materials and Methods

3.2.1.1. Synthesis of GO

Bulk graphite (Sigma Aldrich Cat# 332461, Lot: MKBK4082V) sieved (420µm, U.S. Standard Sieve Series No. 4, Humboldt, Chicago) and collected and SP-1 Carbon (Bay Carbon) was purchased and used. Table 1 outlines differentiators in oxidation protocols used herein and relates them to previous works. Both IGO and HGO were washed with HCl and De-Ionized water until sulfate free. To summarize results we have labeled samples of GO and rGO samples by their respective oxidation and parent graphite size and source, i.e. I3, I4, refers to IGO-30 and IGO-450 respectively.

3.2.1.2. Reduction of GOs

GOs were reduced in a method using L-AA reduction described elsewhere [98]. Briefly, 0.1 mg/ml solutions of GO were prepared by sonicating graphite oxide in De-Ionized water for 60 minutes and adjusted to a pH of 9 using % 25 wt. aqueous ammonia. L-Ascorbic Acid (Sigma Aldrich) was added to solutions to a final concentration of 2 mM. Solutions were reacted at 95ºC for 15 minutes and then recovered by vacuum filtration, rinsed thoroughly with De-Ionized water and dried overnight. Solutions were recovered by vacuum filtration, rinsed thoroughly with De-Ionized water and dried overnight. For the remainder of the article rI4 would refer to reduced IGO-450.

3.2.2. Characterization

Fourier Transform Infrared (PerkinElmer, Spectrum-100) was performed using on samples of graphite oxide and reduced graphene oxide that had been vacuum dried at 60ºC for 24 hrs. Thermal Gravimetric Analysis (Mettler Toledo, TGA/DSC) was performed using a heating rate of 10 °C/min from 25°C -800°C. All samples were measured in Alumina crucibles with a volume of 0.7 µl under Argon. Raman (WITec, alpha 300R) measurements were performed using a laser excitation was 532 nm (Nd:YAG). Atomic Force Microscopy (NT-MDT, Ntegra,) was performed in Tapping Mode on samples applied to mica disks (Ted Pella) by drop coating (0.005mg/ml) and drying overnight. X-Ray Diffraction (SIEMENS D5000 X-Ray Diffractometer XRD) was taken of GO papers using a Cu Kα (λ = 0.154443 nm) with start angles of 5 degrees and stop angles of 50 degrees. Hall probe (Ecopia, HMS-300) measurements were performed on rGO papers prepared by vacuum filtration on 0.1µm cellulose ester membranes (Sterlitech) and dried at 80ºC overnight.

3.3. Results and Discussion

3.3.1. Characterization

3.3.1.1. GOs

We compared results from Thermal Gravimetric Analysis (TGA) and Fourier Transform Infrared (FTIR) to investigate oxygen functionalities present in graphene oxide samples recovered after oxidation and purification. According to results from FTIR (Fig. 3. 1.A), all the samples reveal the presence of hydroxyl group OH stretches at 3000 cm^{-1}, carboxyl C=O stretching at 1740 cm^{-1}, vibrations from aromatic sp^2 C=C stretching at 1400 cm^{-1} and ether C-O-C stretching vibrations at 1240 cm^{-1} in. I3 and H3 have additional 1650 cm-1 peaks which signify additional hydrogen bonds between carboxyl groups.

TGA analysis shown in Figure. 3.1. B. are summarized in Table 3.2. as mass loss between 150ºC-400ºC to estimate oxygen functionality [98] derived from equation (1.) using methods previously described by authors [93] and indicated the degree of oxygen functionalization was I4 > H4 > H3 > I3.

$$Mass\ \% = [(Mass\%_{400C} - Mass\%_{150C}) * 100] / (Mass\%_{150C}) \quad (1)$$

Epoxy and hydroxyl functional groups resulting from oxidation of the basal plane have lower mass compared to carboxylic groups functional groups on GO edges that have higher mass. Moreover, this is not really and interpretation for the degree of oxygen but an estimate intended to disregard the water content. Above 700ºC, I3 rapidly loses weight approaching 0% wt. while H3 remains above 15% wt. respectively. I4 has more than 20% wt. and H4 has ~40% remaining mass signifying the stability of the carbon structure is largely influenced by graphite size while water interlamellar intercalation could be a consequence of oxidation and functional groups that are less stable.

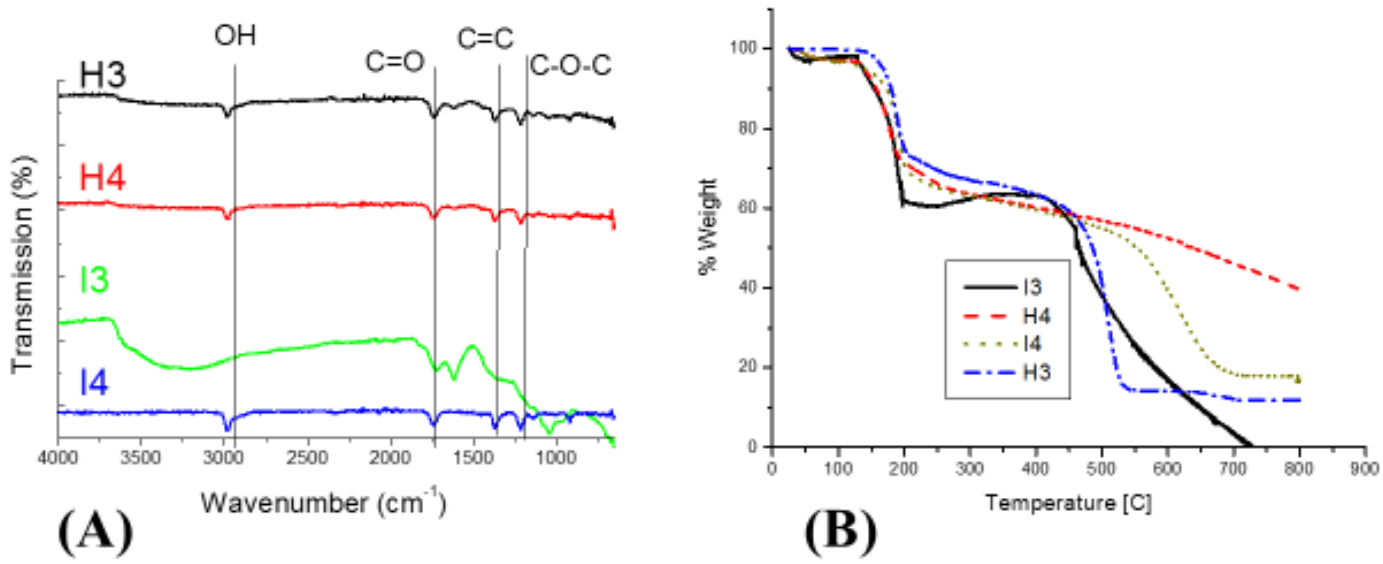

Figure 3.1. Fourier Transform Infrared spectroscopy of graphene oxides (A) and Thermal Gravimetric Analysis (B) of graphene oxides.

X-Ray diffraction patterns (XRD) in Figure. 3.2 taken of GO papers illustrate differences in interlayer spacing as well as GO crystalline size. Interlayer spacing distance is further summarized in Table 3.3. show *d* is above <0.7 nm for all samples due to oxygen groups observed with FTIR and water intercalation.

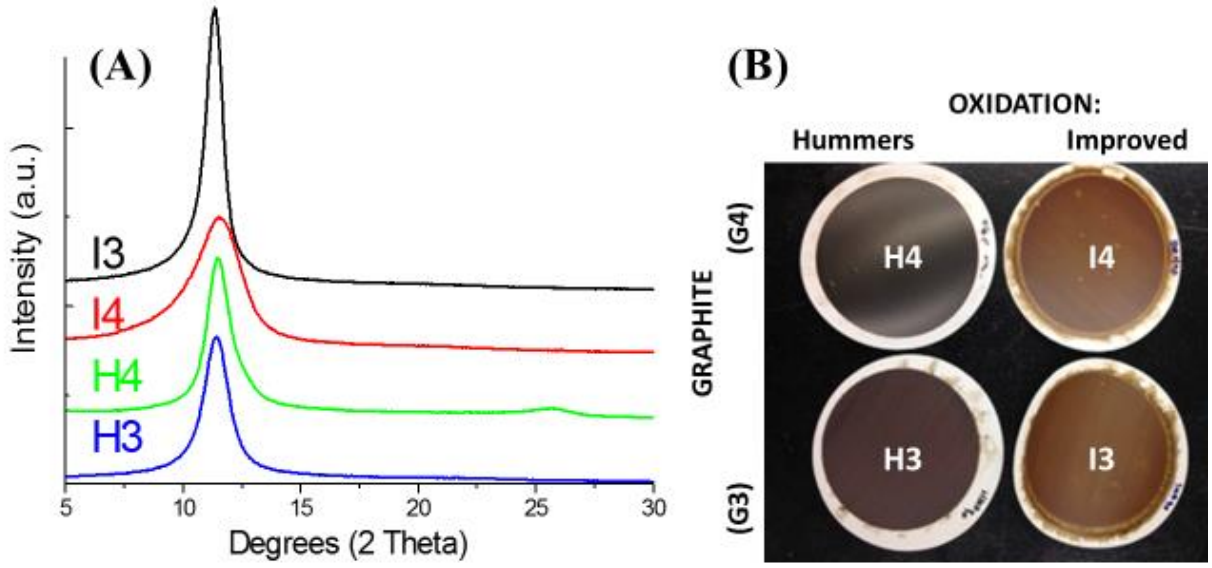

Figure 3.2. X-Ray Diffraction patterns of graphene oxide papers (left) digital image of graphene oxide papers (right).

I3 and H3 have less mass loss but more inter-lameller spacing than I4 and H4 but that are a possible result of hydrogen bonding between edge smaller sheets and edge carboxyl groups. H4 had identical *d* spacing to H3 and a very similar mass loss between 150-400ºC compared to I4 and I3 which showed a noticeable difference in mass loss and interlayer spacing. H4 is the only sample to have a peak remaining from the 002 plane of its parent graphite (Figure 3.2.). The pH of each solution (0.1 mg/ml) was taken before neutralization and addition of the reducing agent and appears to show no correlation to either interlayer spacing or oxygen content. However, HGOs are lower in pH than the resulting IGO samples and Hummers method has been reported to produce oxidative debris such as humic and fulvic acid [91] and could explain such similarities in *d* spacing and oxygen mass loss between H3 and H4 samples when compared to I3 and I4 samples, despite the differences in parent graphite size.

Table 3.2. pH of GO solution (0.1mg/ml) and TGA data.

Sample	pH	Mass loss 150°C - 400°C
I3	2.95	30.8
H3	2.86	34.7
I4	3.30	36.7
H4	3.00	35.5

The Scherr equation was used to estimate the number of layers of graphite precursor to the corresponding GO crystallites [93]. We fit the full width at half peak maxima (FWHM) using Lorentzian fitting to determine (002) and (100) peaks and utilized these measurements for the determination of Lc and La using Scherrer formula [94-96]. Table 3.3 summarizes the 2 theta maxima, fwhm, Lc, d, and La data for the graphite precursors and GO samples.

Table 3.3. 2 theta maxima, fwhm, Lc, d, and La from X- Ray Diffraction measurements.

Sample	2Θ	d (Å)	FHWM $(^o)_{002}$	L_c (nm)	FHWM $(^o)_{100}$	L_a (nm)
G3	27.04	3.29	0.64	12.82	2.60	6.74
I3	11.33	7.80	0.93	8.52	4.68	3.71
H3	11.43	7.73	1.33	6.02	6.33	2.76
G4	27.21	3.27	0.45	18.36	0.71	24.59
I4	11.55	7.65	2.60	3.07	4.16	4.19
H4	11.43	7.73	0.63	12.66	1.24	14.06

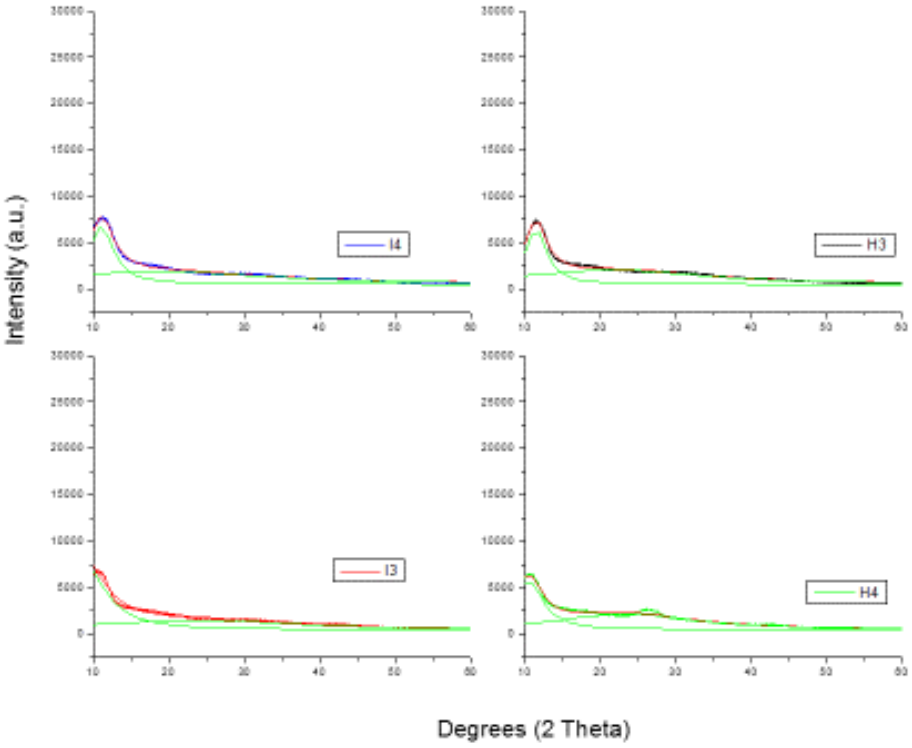

Figure 3.3. Lorentzian fitting of (002) and (100) peaks from X- Ray Diffraction of synthesized Graphene Oxides

AFM images and height profiles show GO thicknesses between 1.4 nm and 1.5 nm indicating single layers were obtained. H4 and I4 show flakes that are in the range of several microns while I3 and H3 show flakes that range from several hundred nanometers.

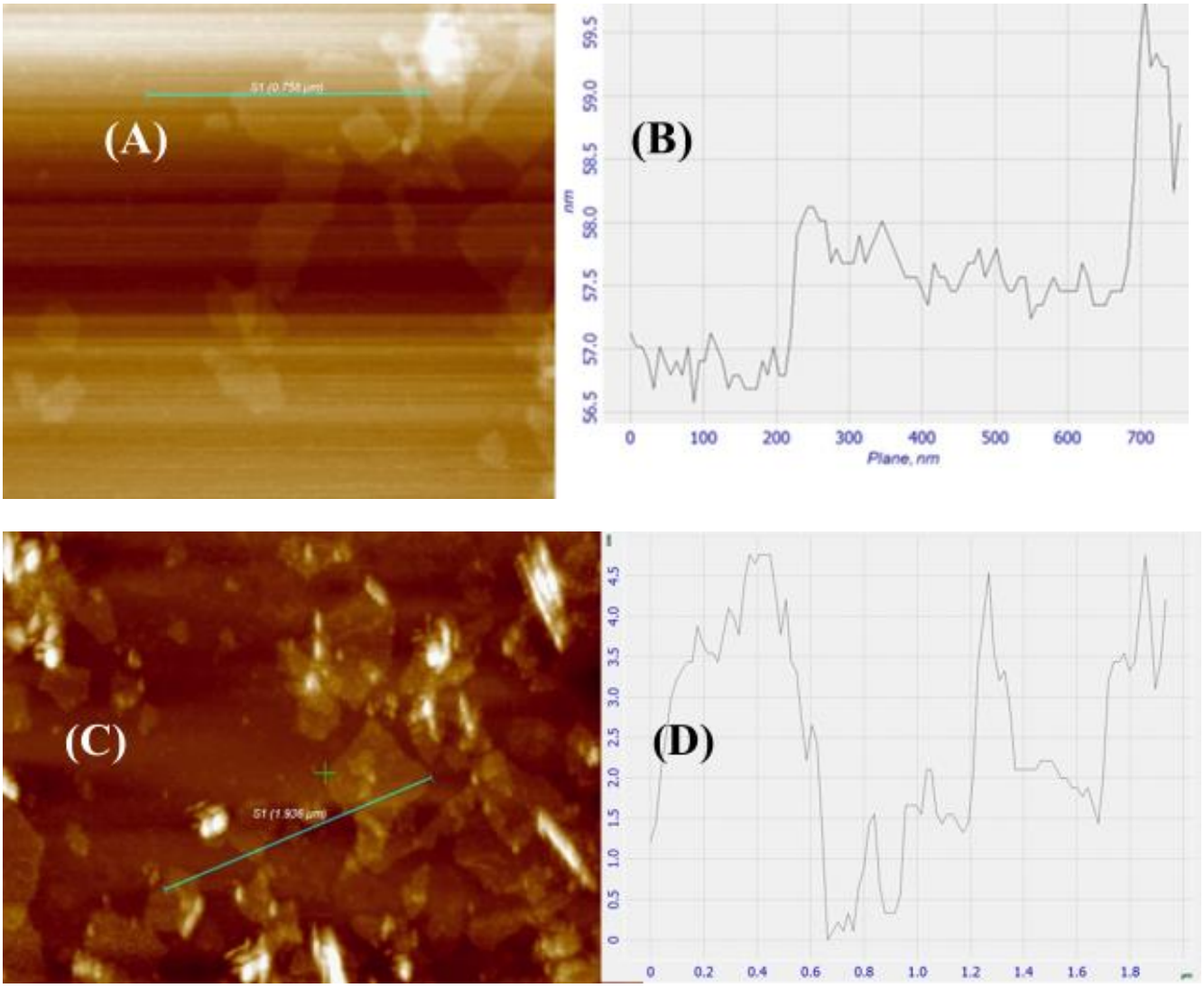

Figure 3.4. AFM images of H3 (a-b) and I3(c-d)

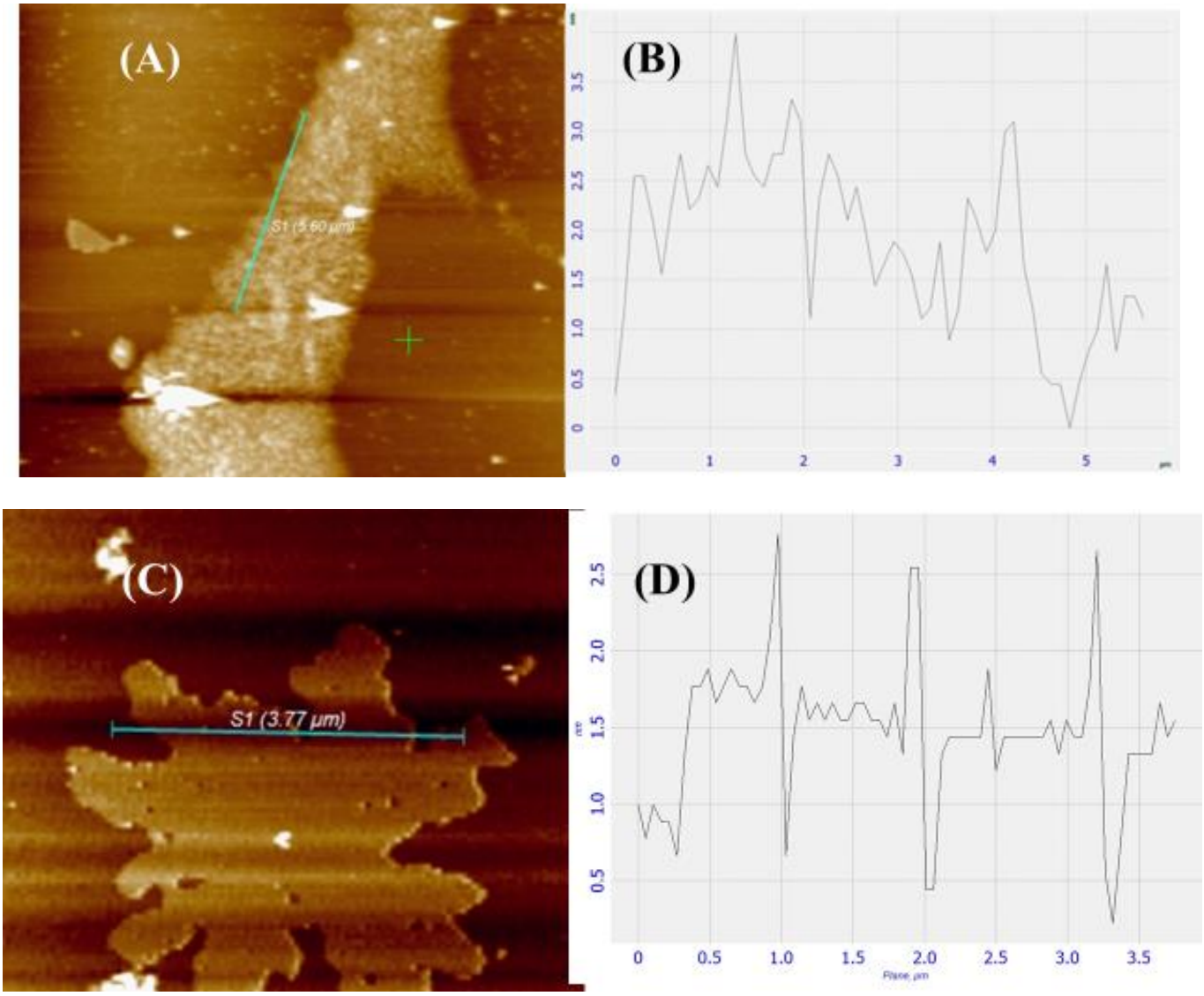

Figure 3.5. AFM images of H4 (a-b) and I4 (c-d)

3.3.1.2. rGOs

FTIR results from samples recovered after the reduction (Fig. 3.6.A.) show the remaining presence of hydroxyl group OH stretches and ether C-O-C stretching vibrations in the IGO samples. TGA data (Fig. 3.6. B.) from these samples show the order of mass loss was rH4 < rI4

< rI3 < rH3 at temperatures above 700ºC, indicating that carbon size dominated carbon structure and stability of resulting reduced products instead of the oxidation. It appears that rH3 has the least amount of residual water, the most stable oxygen groups but the least stable carbon skeleton compared to rI3. This observation could indicate that the quantity of stable the oxygen functionalities present in the GO can determine the amount of damage is done to the remaining sp^2 hybridized carbon structure during reduction. Most likely this order of mass loss correlates to more carboxyl edge groups in H3 and in I3 and demonstrates when using a smaller parent crystalline graphite size, the advantage of phosphate groups stabilizing basal plane oxidation and subsequent reactivity is more pronounced while the effects are less pronounced when using a larger parent crystalline graphite size.

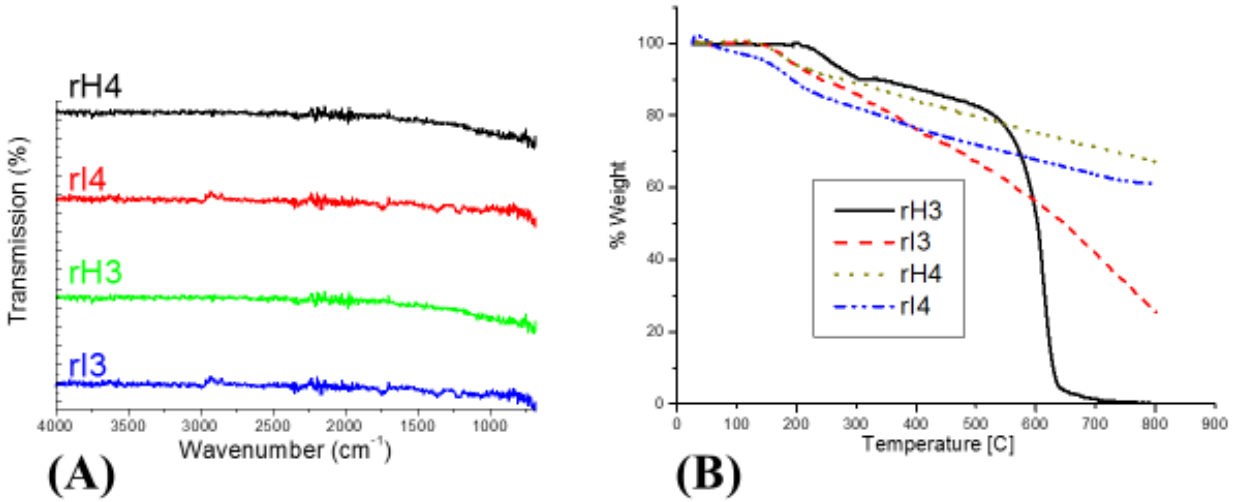

Figure 3.6. FTIR (A) and TGA (B) results from first reduction

Raman spectra of reduced graphene oxide papers are shown in Figure. 3.7. Peaks shown at 1350 cm^{-1} and 1595 cm^{-1} respectively are consistent with the D (sp^3 hybridized carbon) and G (sp^2 hybridized carbon) band. Higher I_D/I_G ratios indicate that more sp^3 hybridized carbon domains are present [88] ad lower ratios indicate more sp^2 hybridized carbon. I_D/I_G ratios were determined to be 1.14, 1.13, 0.95, 0.66 for rH3, rI3, rI4 and rH4 respectively. The I_D/I_G ratio for rI3 is lower

than rH3 which is consistent with previous findings [92] [96], but only slightly despite mor

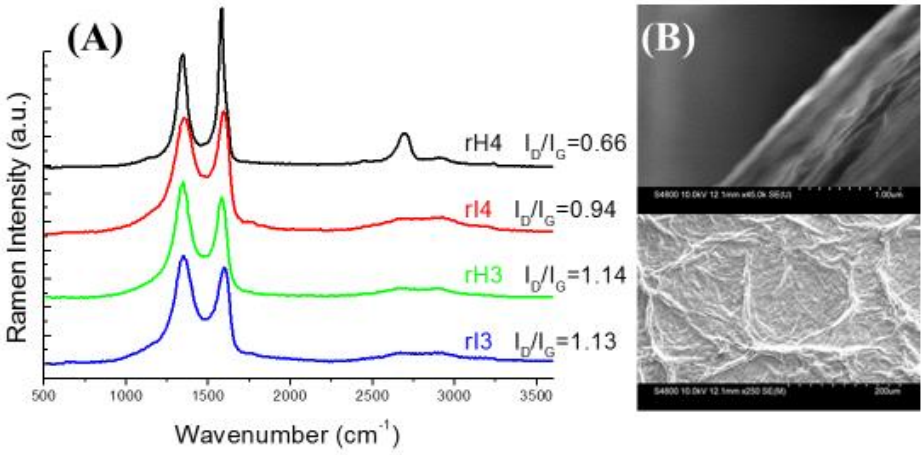

Figure 3.7. Raman Spectra (A) of rGO papers and SEM (B).

extensive oxidation. In contrast, when using a larger parent graphite there is a more pronounced difference between oxidation protocols and it can be seen here that Mercano-Tours effective oxidation protocol has compromised the sp^2 hybridized structure in rI4 by while rH4 has the presence of a 2D peak and a very narrow G peak showing it retains graphitic structure and symmetry.

3.3.2. rGO paper performance

Although rI4 and rH4 were synthesized from the same parent graphite and reduced under identical conditions, Hall probe experiments summarized in Table 3.4**.** show rH4 exhibits a conductivity two orders of magnitude higher than rI4. Interestingly rI4 had a conductivity extremely similar to rI3 despite the different parent graphite and subsequent GOs shown from the

TGA, suggesting that the oxidized regions evidenced from FTIR have more influence on restoring conductivity than areas of ordered conjugated sp^2 carbon.

Table 3.4. Comparison of rGOs produced from different methods in comparison to literature

Ref	Sample	Reducing agent	Conductivity (S/cm)	300°C anneal in Ar/H	900°C anneal in Ar/H
#99	HGO	Hydrazine	0.05	2.1	375
#99	HGO+	Hydrazine	0.05	6.8	350
#99	IGO	Hydrazine	0.1	3.5	400
Present work	rI4	L-AA, NH_4^+, 95C-15min	0.51		
Present work	rH4	L-AA, NH_4^+, 95C-15min	52.6		
Present work	rI3	L-AA, NH_4^+, 95C-15min	0.53		
Present work	rH3	L-AA, NH_4^+, 95C-15min	16.7		
#98	rGO-V4	L-AA, NH_4^+, 95C-15min	77		

Raman indicates that rI4 and rI3 have little difference between them compared to rH3 and rH4 samples and confirms the similarities in structure despite graphite source and respective GO characteristics. Papers produced with rH4 exhibits ~ 3:1 increase in conductivity in comparison to rH3 papers due to larger flake size and less inter-sheet contact resistance, consistent with results previously reported [73]. GO monolayers produced from the improved oxidation method and reduced with hydrazine vapor were about twice as conductive (~ 10 S/m) as reduced GO made using hummers method. However the authors of the study also found it was not sufficient to achieve high conductivities without annealing, which eliminates most of the differences in structure and composition between samples. As a result, it was difficult to conclude whether or not hydrazine reduced IGO flakes are indeed more conductive than HGO counterparts [99]. It has previously been shown that L-AA reduction imparts less disorder than rGO prepared from hydrazine [100] largely due to surface adsorbates that stabilize L-AA reduced GO in solution.

Our first reduction reaction was 15 minutes with the aims of minimizing these adsorbates but they may be responsible for functionalizing IGO samples and could explain similarities in conductivities. However, since all the samples can be considered reactive with these adsorbates, the results can be used to understand what influence GO reactivity has on subsequent reduced structure. We carefully controlled the sonication time (3hrs) when preparing GO sheets in solution to minimize sheet size reduction [86] and consequent oxidation. We chose not to reduce the samples further either chemically or thermally so as to appreciate fully the intrinsic properties of sp^2 hybridization of carbon that are present before and after chemical reduction. While the samples were not further reduced, rH4 samples were more conductive than samples reduced using hydrazine [100],[89] metal acid [101],[102] or metal alkali [103] and other organic compounds [104-106]. All the samples from the first reduction were as conductive or more conductive than previous accounts of GO reduced by Sodium Borohydride [107-109] so we found that our methods were capable of providing data that would demonstrate the qualities of the oxidation and reduction with respect to graphite source and size. Overall, when using L-AA as a reducing agent in solution, these results show extensive oxidation in Marcano–Tour's method makes reduction more difficult which has been previously reported [92].

3.4. Conclusion

Our findings reveal that extensive oxidation results in GO products similar in functionality that are less influenced by the graphite source or starting size. If the oxidation protocol is less aggressive products are largely dominated by graphite source and size consequently determines reactivity during reduction. When restoring electrical conductivity, this work illustrates the importance of investigating not only the size and starting graphite but also

the importance of comparing oxidation protocols. It is important to prepare well oxidized graphite oxide as a starting material when using GO in solution but care must be taken not to produce a more reactive GO that will be harder to reduce and restore to a conjugated state.

While there is progress in graphene research and application, it commercialization is still in the developing stages. Understanding the influence oxidation and parent graphite have on synthetic chemical methods is important to understand for reducing, functionalizing and producing high quality graphene. These results can aid in the development of materials used in transparent conductive layers for solar cells, transparent electrodes, coatings, sensors and other nano-electronic devices from low cost chemically derived graphene. This work can be useful for material scientists and aid synthetic chemists that are interested in the role graphite source and oxidation path have on determining the quality of resulting reduced graphene. It can further demonstrate the importance of carefully selecting and controlling synthetic methods when producing large amounts of graphene oxide in solution from graphite oxide.

Chapter 4: TRANSITION METAL DOPED GRAPHENE FROM PETROPORPHYRINS

4.1. Background

The electronic and magnetic properties of graphene can be modified through combined transition-metal (TM) and nitrogen decoration of vacancies. Additional modes of functionalization that are currently being explored for a wide range of applications in nanoelectronics [108-110], spintronics [111] and electrocatalysts [112,113].

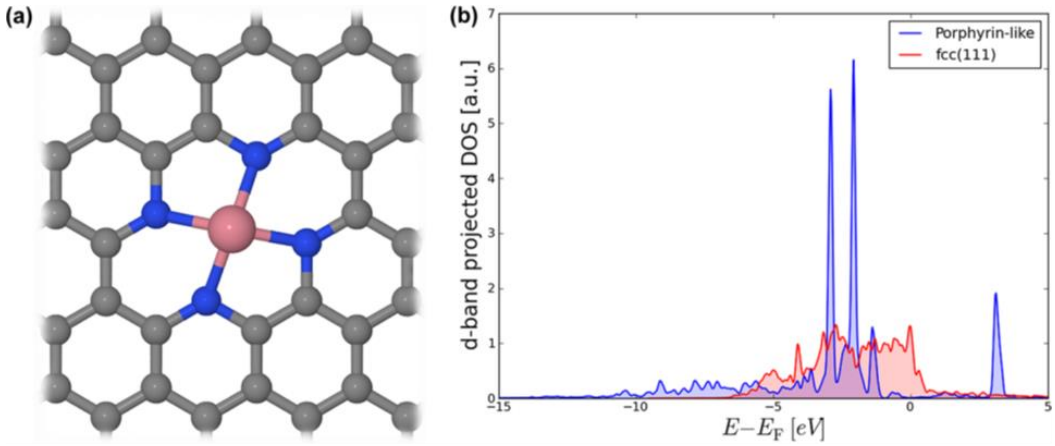

Illustration 4.1. (a) Atomic structure of porphyrin-like functionalized graphene. The central metal atom is coordinated to four nitrogen atoms, forming the porphyrin ring that is embedded in a graphene matrix. (b) Comparison of density of states projected onto the d orbitals of the Fe atom located at the center of the porphyrin ring and the Fe surface atom in Fe (111) face center cubic surface [112].

Researchers previously discovered that TMs bind to graphene strongly in a four nitrogen configuration [115]. The stability in the presence of the defects associated with TMs can be attributed to the reduced electrostatic repulsion between nitrogen lone-pair electrons due to the hybridization between N and TM. Results from DTF studies have predicted these types of structures to be particularly promising candidates for graphene-based ferromagnets, which could find applications in nanoelectronics and nanomagnetism.

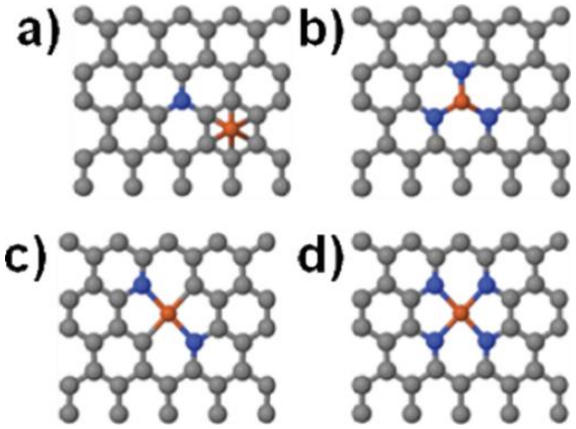

Illustration 4.2. (a) TM-adsorbed N-doped graphene, (b) TM−N3 defect, (c) TM−N2 defect, and (d) TM−N4 defect configurations. Gray, carbon; blue, nitrogen; brown, cobalt or iron [115]

Graphene-type molecules, typically large polycyclic aromatic hydrocarbons (PAHs), have gained enormous interest because of their unique self-organization behavior and promising electronic properties for applications in organic electronics [116]. Asphaltene is a part of crude oils that contain a large number of structures, in specific high molecular weight bonded PAH components with hetero-atoms. Asphaltene appears brown or black in color, and the melting point differs with oil geographical sources [117]. The definition today is similar; it is insoluble in n-alkanes, such as n-pentane or n-heptane, and soluble in toluene [118]. Asphaltene extracted using n-

pentane known as C5-Asphaltene and with n-heptane known as C7-Asphaltenes. The amount, chemical composition, and molar mass distribution of the Asphaltene "solubility class" vary significantly with the source of the crude oil and with the method of precipitation [119-123].


(a)
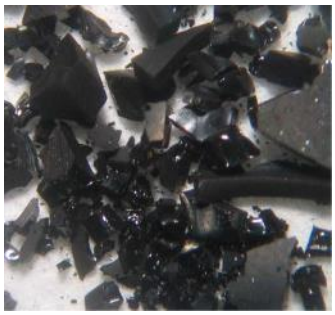
(b)

Illustration 4.3. Asphaltene extracted by (a) n-pentane (b) n-heptane

Several metals (e.g., Ni, V, Fe, Al, Na, Ca, and Mg) shown to accumulate in the asphaltenes fraction of crude oil, typically in concentrations less than 1 % w/w [124-126].
Vanadium and nickel, the most abundant of the trace metals, present mainly as chelated porphyrin compounds, and they linked to catalyst poisoning during upgrading of heavy oils [127,128]. The concentrations of other trace metals not bound in porphyrin structures (e.g., Fe, Al, Na, Ca, and Mg) indicated to change in deposits as a function of well depth [129], and amongst sub fractions of asphaltene.

The Army Research Laboratory and Defense Advanced Research Projects Agency (DARPA) funded a four year study to modify graphene and produced an entirely new material spun out of boron, nitrogen, carbon, and oxygen that shows evidence of much sought-after thermal properties as well as magnetic, optical, and electrical properties. It shows potential for doped graphene in applications ranging from 20-megapixel arrays for cellphone cameras, photo

detectors or atomically thin transistors that when multiplied by the billions could fuel computers [131].

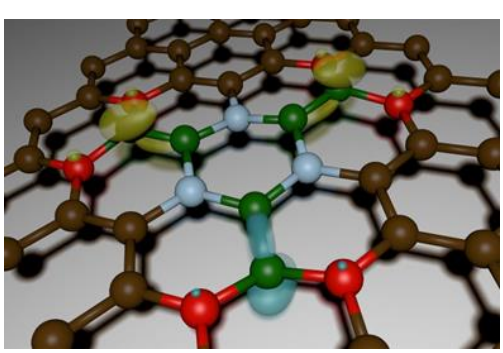
(a.)

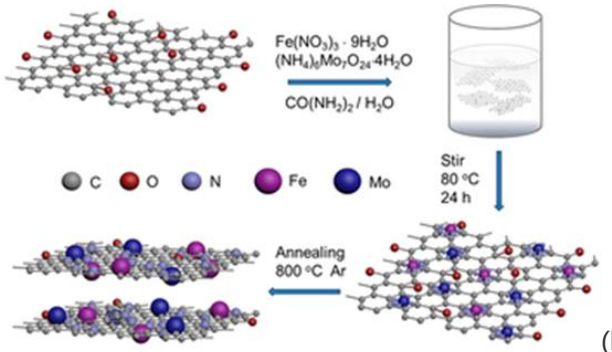

(b.)

Illustration 4.4. An artistic rendering of novel magnetism in 2D-BNCO sheets (a.)[130] and schematic illustration for preparation of iron- and molybdenum- containing nanoparticles dispersed on nitrogen-doped graphene (b) [132].

Herein, we explore the potential to dope graphene with TMs as an alternative to exfoliated, chemical derived [132] and high energy e-beam based methods by using n-alkane extracted asphaltenes.

4.2. Experimental Methods

4.2.1. Materials and methods

4.2.1.1. Asphaltene extraction:

Asphaltene materials were extracted from crude using different n-alkanes and dissolved in toluene for deposition. Asphaltene/toluene (1 mg/ml) solutions were then deposited using drop coating and later spin coating (500 rpm and 1000 rpm for 60 sec) onto previously prepared copper foil.

4.2.1.2. Annealing:

A 4" tube furnace was used to anneal the material under a reducing environment (H2). The system was equipped with a turbo pump with a direct line-of-sight to the sample substrate allowing base pressures below 10^{-8} Torr. To reach high vacuum, not only is a turbo pump used and all the flanges on the high vacuum side of the system are conflat flanges; capable of achieving ultra-high vacuum (UHV). Reaching lower background pressures allows the removal of undesired residual gasses like water and oxygen from the system before growth which can etch graphene at high temperature. The turbo pump also allows the system to reach pressures low enough (below 10^{-5} Torr) to use a residual gas analyzer (RGA). In a typical growth, the sample was loaded into the furnace and allowed to pump down using the turbo pump for two hours prior to heating and gas flow.

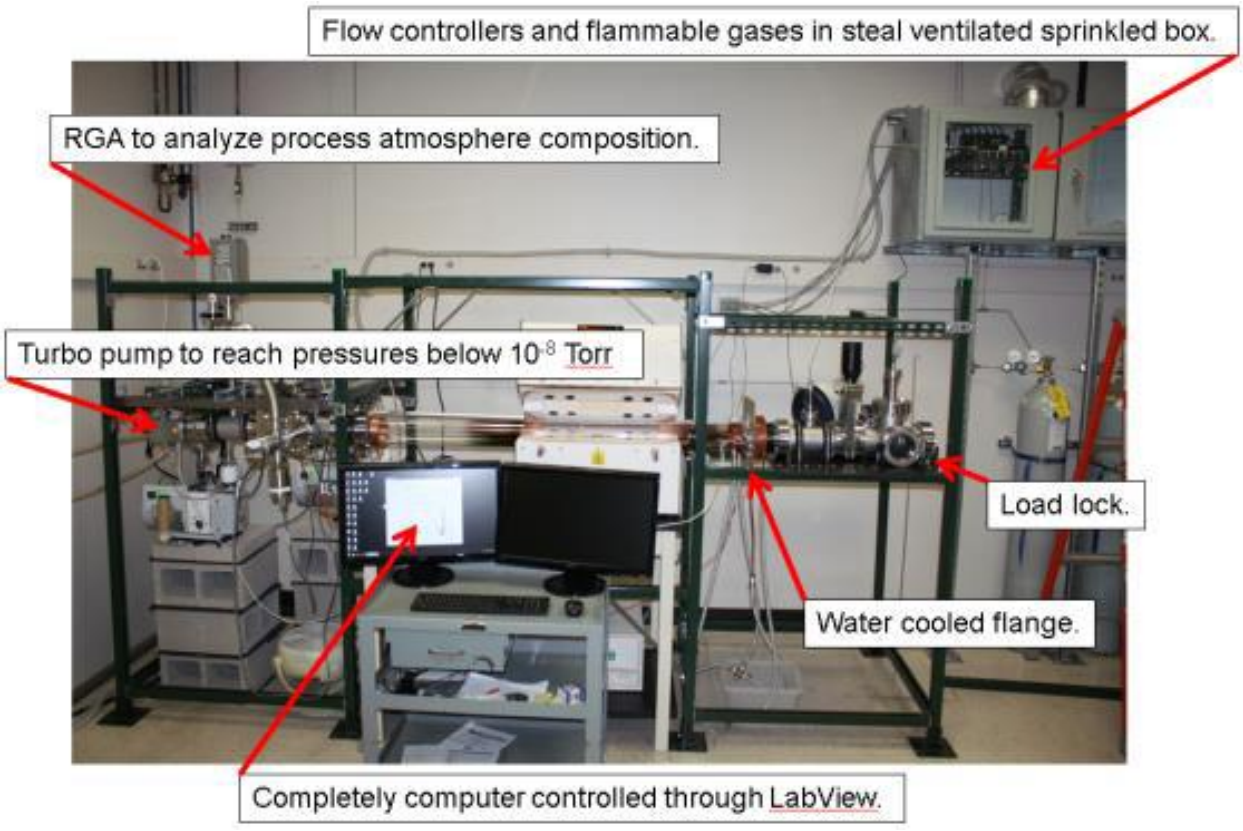

Illustration 4.5. CVD set-up at the J.J. Pickle Research Center Austin, TX

Table 4.1. Experimental conditions and parameters and (above) figure of furnace used in experiment

Experiment	Temperature [^{o}C]	Time [min]	Material	Deposition SC - Spin coated DC- Drop coated	Gas
A	1050	5	Synthetic, C7,C9	SC	*H (10ccm)
B	1050	5	C7	DC	H (10ccm)
C	1050	5	Synthetic	DC	H (10ccm)

*heated to 900C for 30 min in air and then ramped to 1050C under 10ccm H

4.1.2. Characterization

Raman was taken using Witec Alpha 300 micro-Raman confocal microscope after graphene had been transferred to SiO2/Si wafers. Scanning Electron Microscope (SEM) Images were take using a FEI Quanta 650 SEM equipped with Bruker EDX system for chemical analysis. Optical Microscope images of asphaltenes were taken on copper foils before and after growth. Transfers were performed by spin coating polymer, dissolving copper foil and transferring graphene to SiO2/Si wafers. Zeiss Axiovert 100A Light Microscope was used to take images of asphaltenes before and after growth.

4.3. Results

4.3.1. Raman:

Conditions for graphene growth were applied for all experiments except for experiment A when hydrogen was shut off for a period of 30 minutes while temperatures ramped to 1050C. During that time the samples were being annealed in air. The resulting averaged Raman from all

experiments show heavy carbonization and some graphitization of the solid carbon source. We were able to find metals in more than one sample of the post growth C7 asphaltene but when hydrogen was used for the entire annealing and growth process, we found that metals disappeared and that the Raman from Figure 4.1. indicates mostly carbon with some graphitization. Only experiment A exhibited the ratio of 2D to G and D peaks that would indicate the presence of quality graphene rather than sp^2 hybridized carbon.

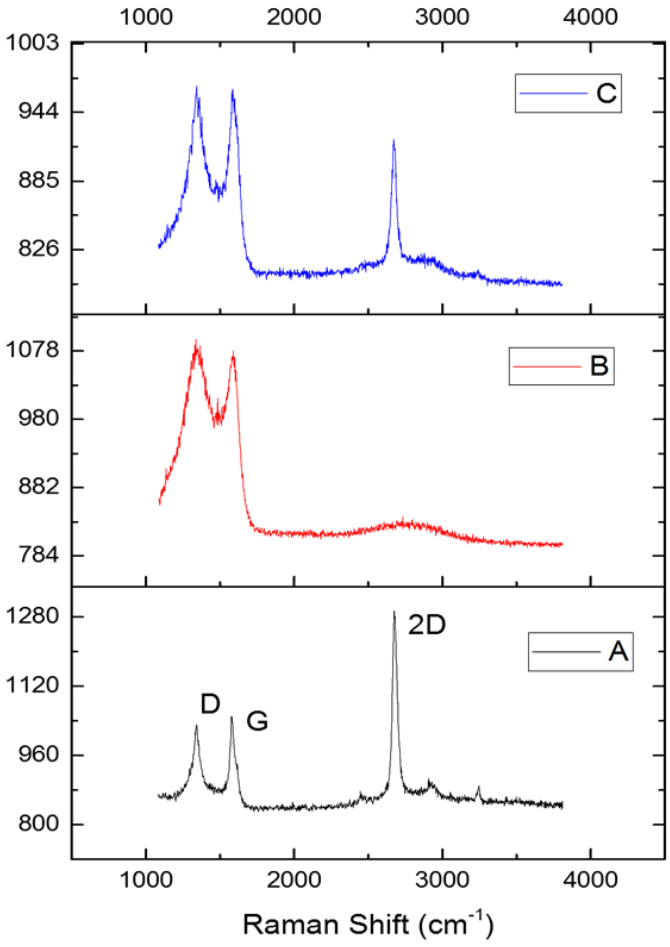

Figure 4.1. Raman summary for experiments

4.3.2. SEM/EDX:

Metals identified in post growth samples from experiment set A and B included Al, Fe, Zr and adatoms included sulfur. EDX analysis was taken of the copper foil before any etching in Figure 4.2. and foil which had been sonicated in acetone before applying asphaltenes shows no metals or adatoms present before growth indicating that metals and adatoms indeed came from asphaltene samples. After growth, Experiment A EDX shows the presence of Aluminum and Iron.

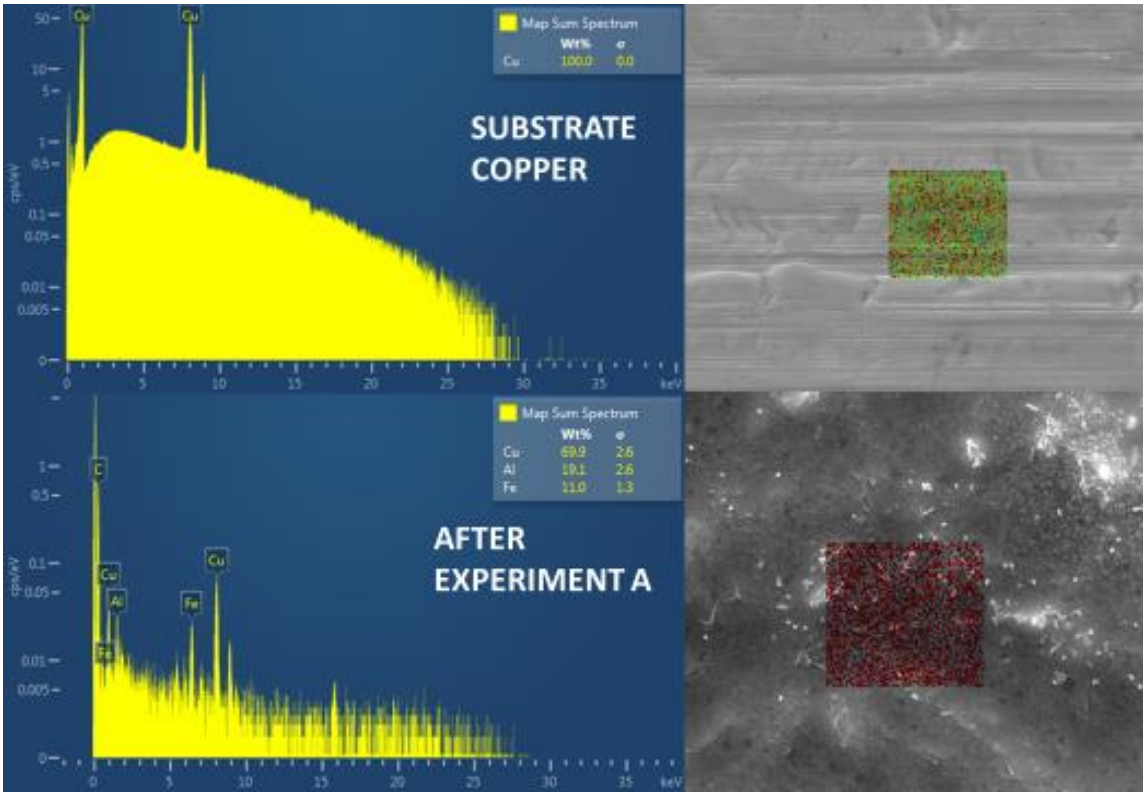

Figure 4.2. EDX analysis (top left) of copper foil sonicated in acetone before application of solid carbon source with corresponding SEM image (top right) EDX elemental analysis respectively (bottom left) from SEM section (bottom right) from C7 in Experiment A

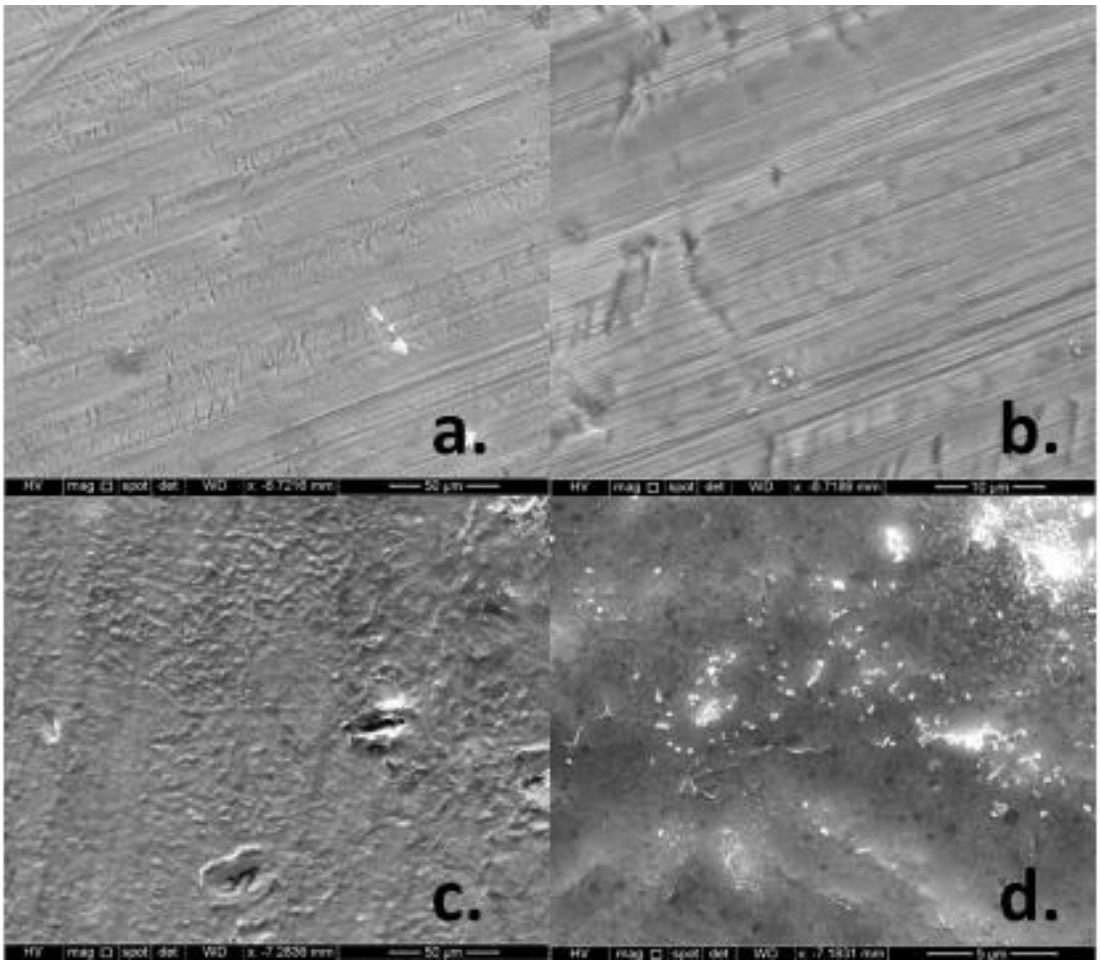

Figure 4.3. SEM images of C7 asphaltene on copper foil before (a,b) and after (c,d,) growth

Experiment B indicated the presence of TMs Iron and Zirconium before growth but Iron disappears after growth conditions.

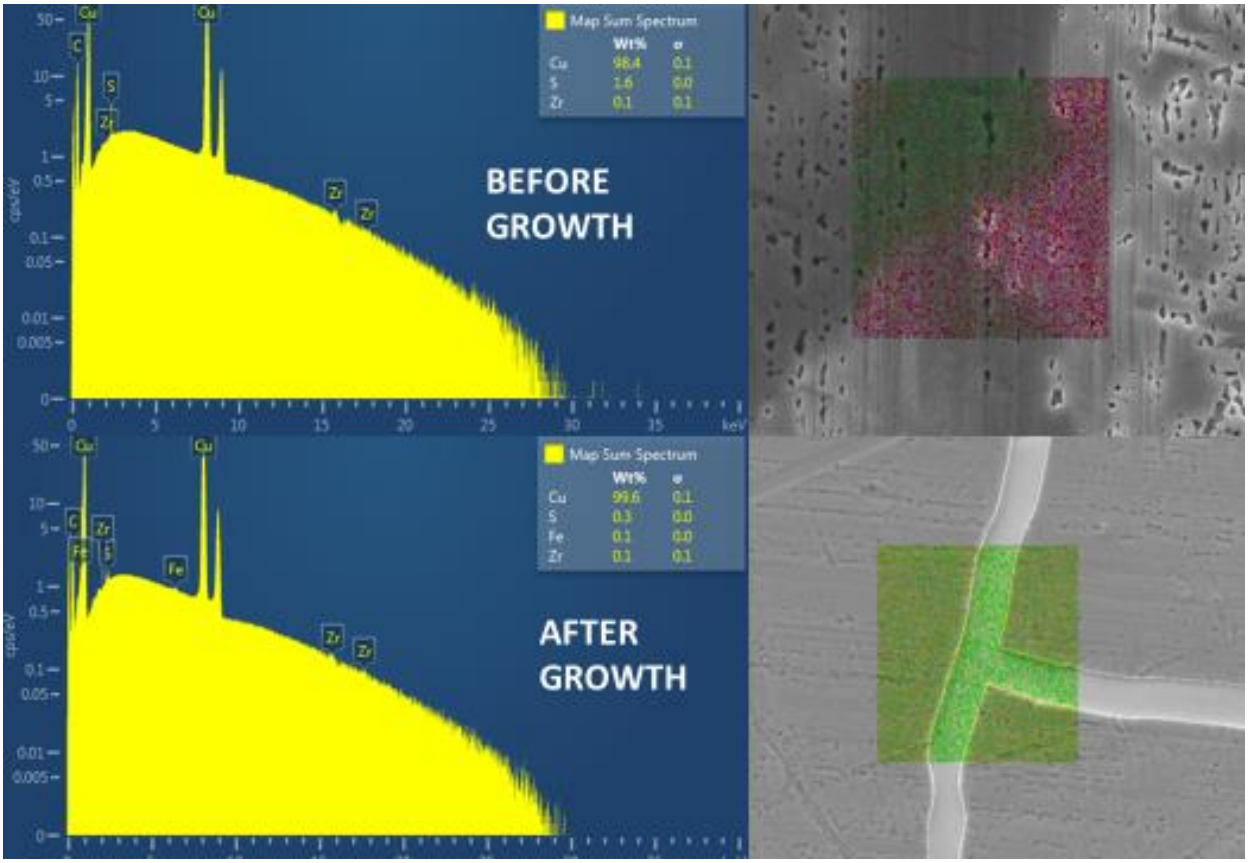

Figure 4.4. EDX (left) and SEM from Experiment B after drop coating (top) and after growth (bottom)

To further study asphaltene adatoms, we took EDX of a synthetic asphaltene containing no metals. Figure 9 shows synthetic asphaltene contained no metals or adatoms after being deposited. Needless to say from data in Figure 4.4. we found no TM or adatoms present after growth.

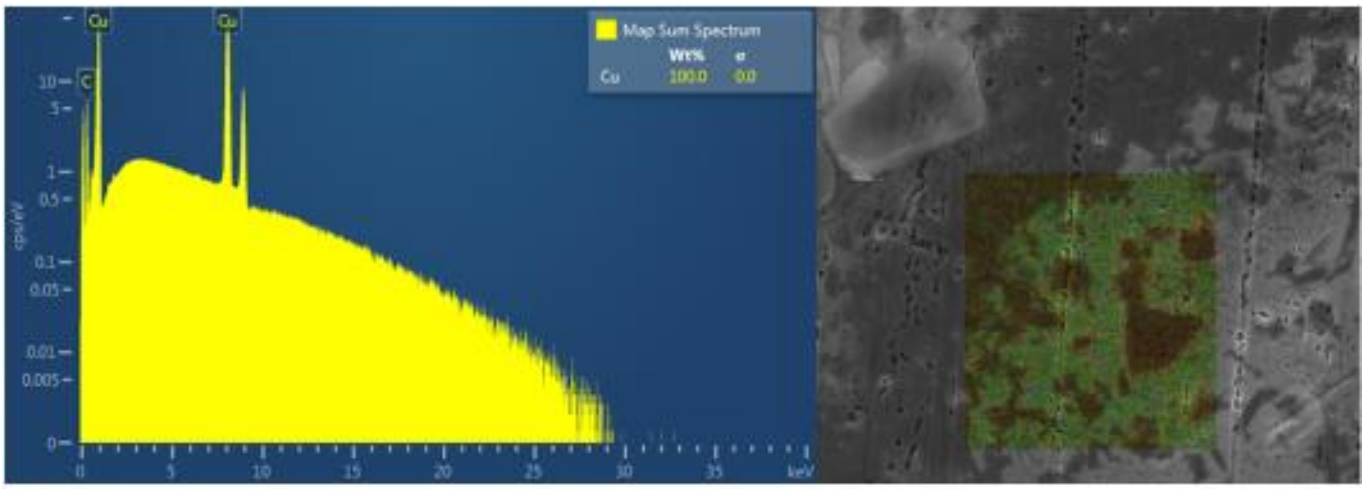

Figure 4.5. EDX (left) from pregrowth drop coated synthetic asphaltene in Experiment C (right)

4.3.3. Optical Microscope:

Pictures taken using OM show copper coated with C7 asphaltenes before and after growth. There are clustered discotic structures before growth and curiously there are areas after growth that show clearly more than a few layers graphitized. There are areas that can be seen where copper can be seen as clear orange from underneath sheets of graphitized carbon in Figure 4.6 (c) and (d).

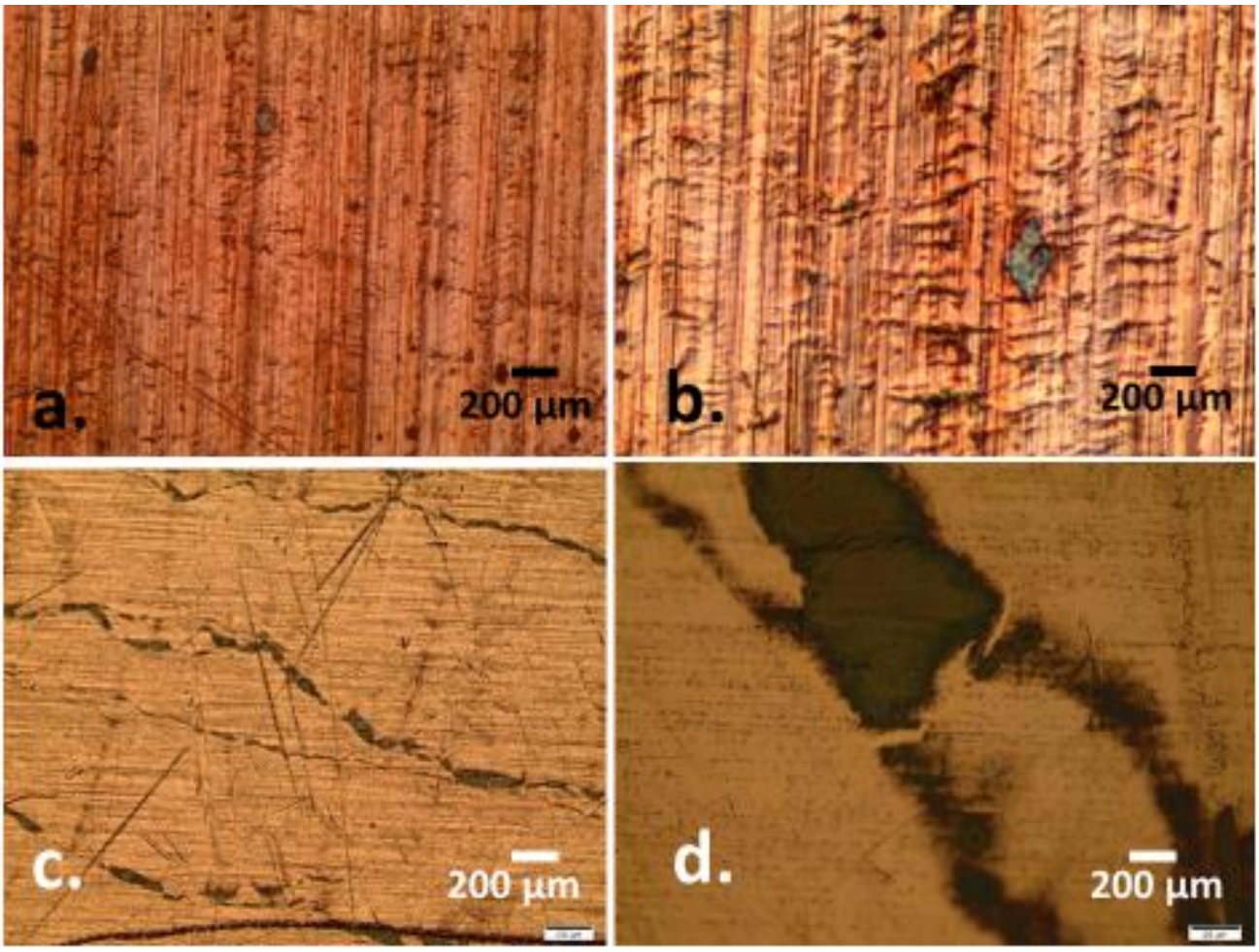

Figure 4.6. Optical microscope images of C7 asphaltene on copper foil from experiment A before (a,b) and after growth (c,d)

Figure 4.7. Experiment A transferred to SiO2/Si wafer with rips and wrinkles.

4.4. Conclusion

Transition metal (TM) adatoms and graphene have recently been a topic of great interest. They are expected to induce novel magnetic and superconducting behavior. There have been extensive theoretical studies because of these interesting properties but the experimental exploration of TM/graphene systems is very limited. Graphene with Boron and Nitrogen (BCN) is a sought after material due to the fact that graphene has no band gap. Graphene in its single crystal form is a conductor, not a semi-conductor, so while it has amazing properties sought after by so many researchers, it has yet to make a significant impact on electronic industries for this reason.

BCN is currently being researched because it can be introduced by vapor. In contrast, TMs cannot be introduced by vapor. Even if they could be introduced at high temperatures, it has been determined that they would not be stable in an in-plan configuration due to the high differences in energy between TMs and carbon. Boron and Nitrogen both neighbor carbon on the periodic table and do not have a large differences in electron structure. Our carbon source generated from waste crude oils is unsuitable for hydrocracking because of the presence of TMs. We were able to utilize that waste as a valuable source of metalloporphyrins for placing TMs directly inside the graphene lattice.

Chapter 5. METALLIC QUANTUM WIRES FROM ASPHALTENE.

5.1. Introduction

The process of surface-assisted cyclodehydrogenation of polycyclic aromatic hydrocarbons (PAHs) recent years has been one of the most effective, versatile, and flexible strategies for the bottom-up synthesis of small graphene flakes (nanographene), and nanoribbons [133-135].

The electrical properties of p- and n-type discotic liquid crystal have been studied after doping them with a small concentration of electron acceptor or donor and found to behave as molecular wires or quasi 1-D wires [136]. Suen *et al*. synthesized carbon nanofibers with a 66nm diameter from coronene using low temperature vacuum sublimation without using catalysts. The found that the molecule self-assembled into columnar aggregates and showed much better thermal stability than commercial carbon nanotubes [137]. De Luca et. al. used solvent vapor annealing to control the self-assembly of different PAHs after spin-coating and drop-casting onto substrates. They found that the SVA approach was capable of mass transporting molecules over distances hundreds of microns leaving behind crystallites reorganized into nano-fibers, needles and domes [138].

Park et. al. studied the formation mechanism of these wires when casted from toluene and benzene solutions. Atomic force microscopy revealed that the discotics spontaneously form very long and thin wires and self-align along a common orientation. They also found that chemical structure of the solvent appears to have a key role, coupling to the liquid crystal self-assembly. However, other aspects of the assembly such the rate of solvent evaporation, and the nature of the substrate can favor or interfere with the self-assembly into long structures. They found the use of solvents with aromatic structure advantageous because it affects the geometry of the assembly and promotes long wire formation, but it is also compatible with good quality of the intermolecular

order and the electrical properties of ordered systems show a clearly higher electrical conductivity compared to the disorganized aggregates [139].

5.2. Experimental

5.2.1. DLCs

Mesophase DLC pitch was extracted from Crude oil (Mayan) by n-alkane (1:40 v/v). The solution was mixed for 24 hours and filtered (Whatman 40). It was dissolved in toluene and filtered again and the solutions was collected and evaporated. 100mg of sample was heated to 500C for 10 minutes in a flask using Schlenk technique and kept under vacuum. We designate A166 as the precursor DLC and A166-HT-10V as the heat treated DLC.

5.2.2. Characterization

Fourier Transform Infrared (FTIR) was taken of samples in KBr pellets (Thermo Scientific). X-Ray Diffraction was taken from 10-60^{o} using Cu Kα λ=0.154 nm at a 0.01 scan step (Bruker). Optical Microscope images was taken of solutions on SiO2/Si and SEM was taken of powder (Olympus). Scanning Probe Microscopy /Scanning Tunneling Spectroscopy was performed on Highly Ordered Pyrolytic Graphite substrates by drop casting solutions (0.05mg/ml) from chlorobenzene. (NT-MDT). Each sample was applied three times independently and measurements were taken of across a line one micron in length with 10 points and cycled for 5 five minutes to ensure a stable scan.

5.2.3. Density Functional Theory Modeling

Our Density Functional Theory (DFT) simulations were carried out using modules available in Materials Studio v. 7.0, distributed by BIOVIA. The proposed structure was built imbedded within an otherwise empty simple cubic cell of lattice parameter 30 Å (in order to approximate a molecular model when using periodic DFT algorithms). The structure geometry

was as an initial approximation optimized using a Forcite force field minimization with a universal force field. The structure's geometry was then further optimized via a DFT method (CASTEP), using a Generalized Gradient Approximation (GGA) with a WC functional (Wu and Cohen, 2006). The electronic Hamiltonian used an energy cutoff of 240.0 eV, a Self-Consistent Field (SCF) tolerance of 2.0 x 10^{-6} eV/atom, a 1 x 1 x 1 Monkhorst-Pack grid for Brillouin zone k-point sampling, and an ultrasoft pseudopotential. After optimizing the geometry of the structure electronic Density of States (DOS) and band structure were calculated using an energy band tolerance of 1.0 x 10^{-5} eV, as well as the same electronic parameters as were used for the geometry optimization of the structure.

5.3. Results

5.3.1. DFT Modeling

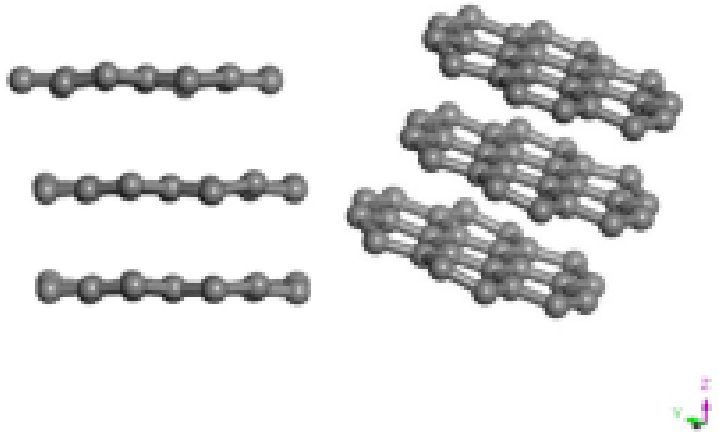

Figure 5.1. Proposed structure for stacked mesophase used in Density Functional Theory experiments

The structure shows that aromatic stacking does increase the density of states at the Fermi energy when compared to a single PAH structure that would represent a quantum dot as can be seen from comparison of DOS for single nano-graphene and three stacked nano-graphenes in Figure 5.2.

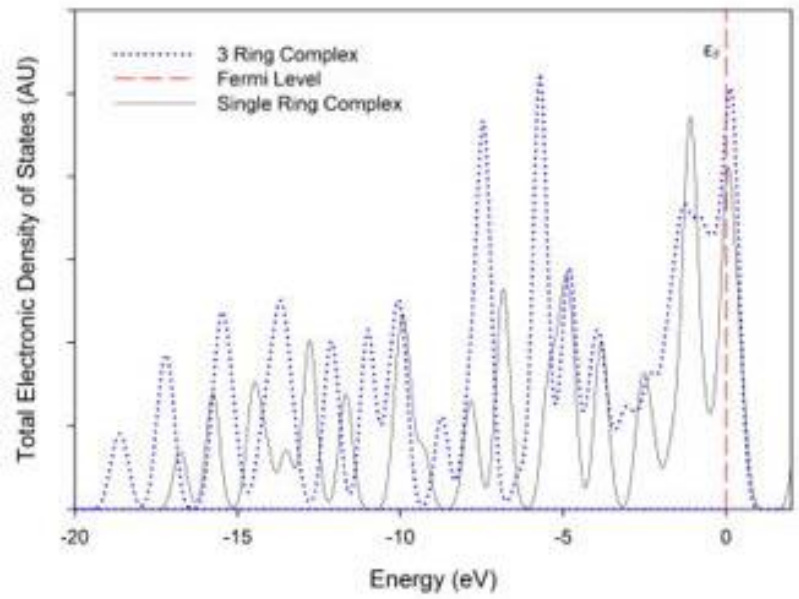

Figure 5.2. DOS plot for single nano-graphene versus the DFT model (blue dotted line) with 3.5 Å separation.

In addition, we compared these findings to calculations from literature of single layer graphene and found our structure to also have a more intense continuous DOS at the Fermi energy than single layer graphene.

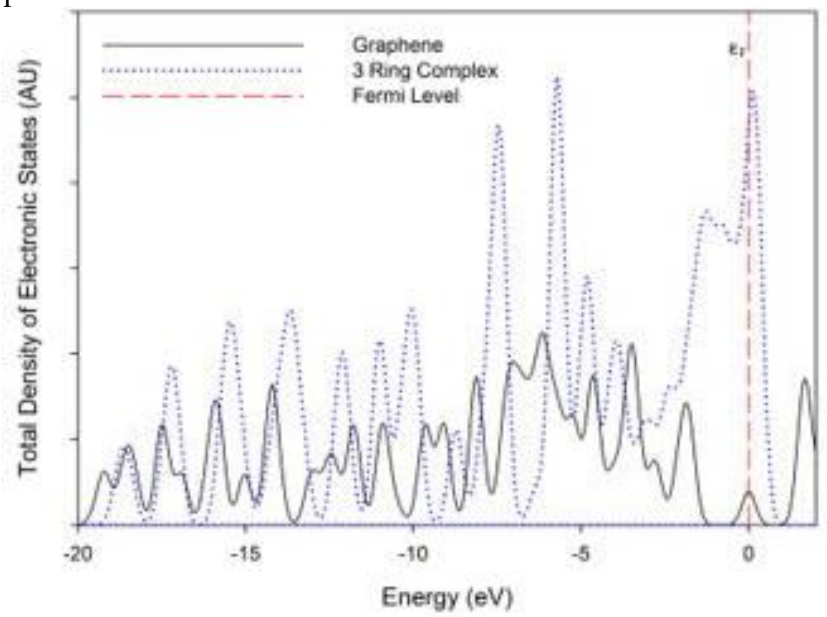

Figure 5.3. DOS plot for DFT model (blue dotted line) with 3.5 Å separation compared to Single Layer Graphene (black line).

5.3.2. Characterization

FTIR shows evidence of cyclo-dehydrogenation as sp^3 carbons are converted to sp^2 carbons there is evidence of akyl group C-H vibrations at 1400 cm^{-1} and C-H stretching from hydrogen or methyl groups attached to aromatics at 2960 cm^{-1} in A166. After heat treatment, sample A166-HT-10 shows vibrations from hydrogens attached to carbons with double bonds at 1100 cm^{-1}, more C=C bond stretching at 1600 cm^{-1} and the total absence of hydrogen attached to aromatic rings. XRD results show heat treatment led to a crystalline structure with ~3.5 Å separation (graphitic π-π stacking) and akyl side chains.

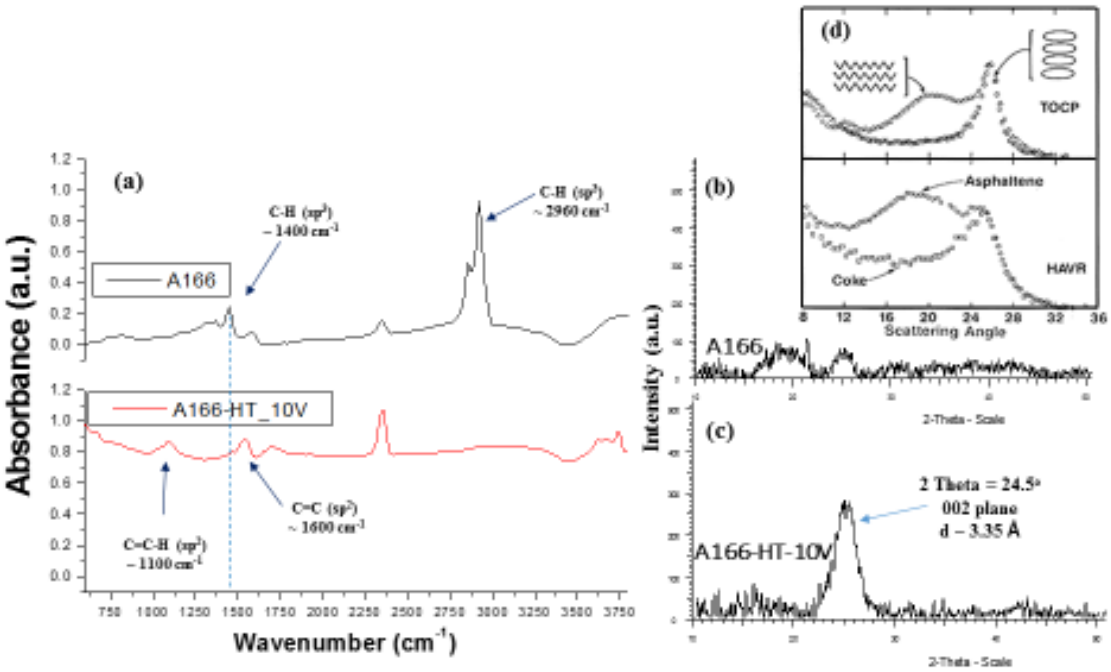

Figure 5.4. Fourier Transform Infrared Spectroscopy (a) and X-Ray Diffraction of A166 (b) and A166-HT-10V(c) in comparison to (d) Asphaltene and TOCP [44].

Optical Microscope images of the samples show A166-HT-10V is much darker than A166 which signifies more layers are present. Samples were spin coated from the same chlorobenzene solutions used for AFM and STM analysis on to Si wafers with 300 nm oxide layer.

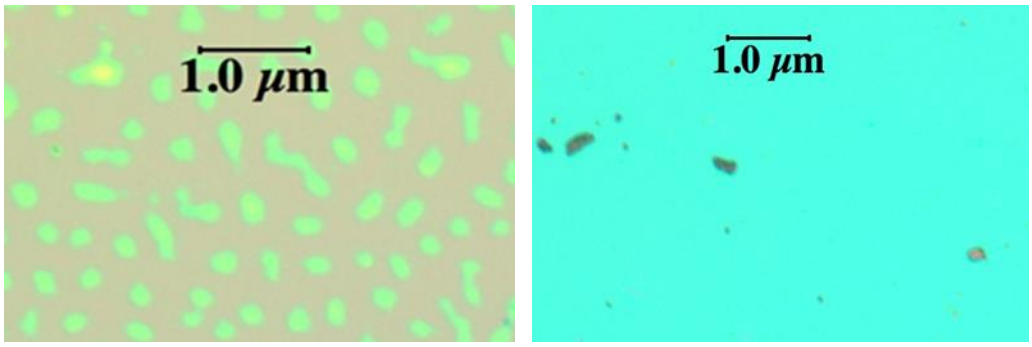

Figure 5.5. Optical microscope from A166 (left) and A166-HT-10V (right).

AFM images prepared from drop casting solutions on HOPG show that A166-HT-10V is distributed in ribbons with more self-association in a unidirectional pattern and A166 shows characteristics of phases without ribbon structures.

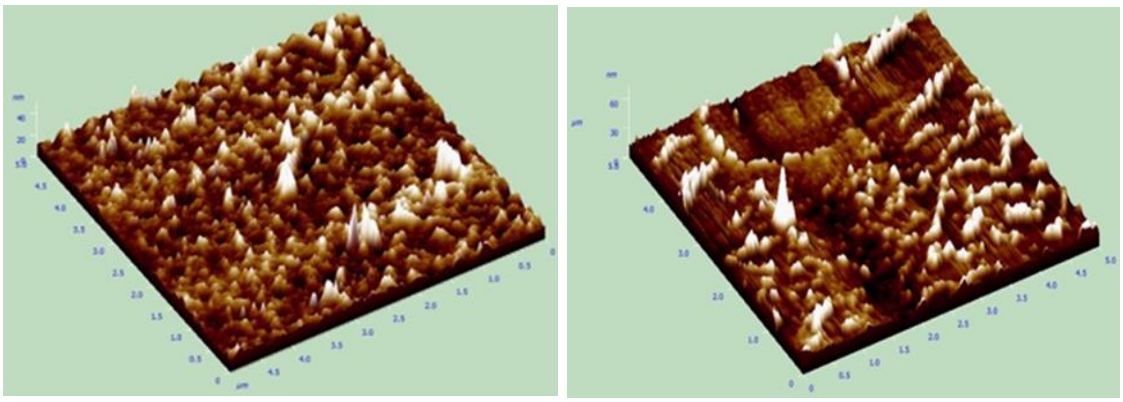

Figure 5.6. Atomic Force Microscope images (5 μm x 5 μm) of A166 (left) and A166-HT-10V (right)

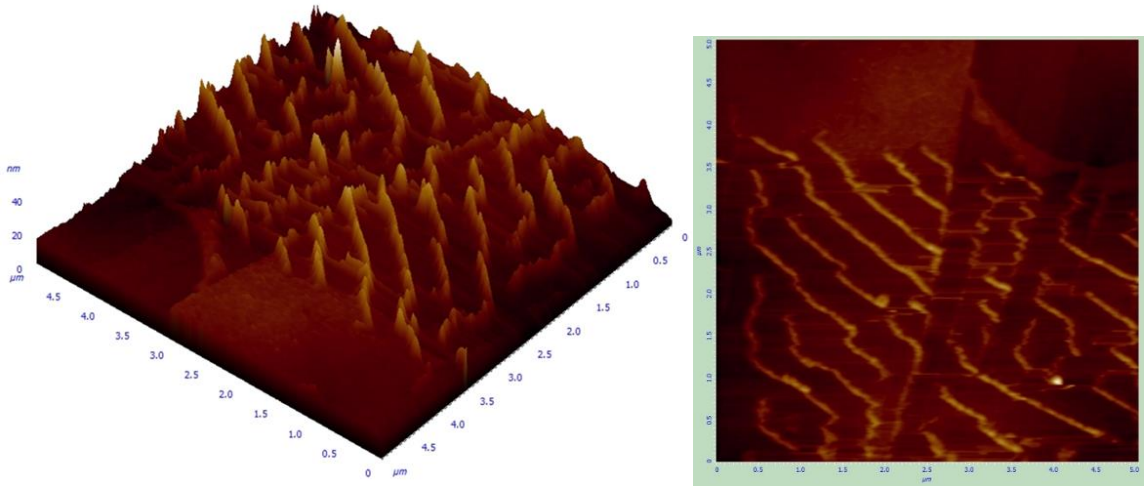

Figure 5.7. Contact Atomic Force Microscope Images (5 µm x 5 µm) of A166-HT-10V

5.3.3. STS Current Voltage curves: I(V) spectroscopy

Scanning Tunneling Spectroscopy taken on the same samples from +1 Volt to -1 Volt indicates that the A166-HT-10V has metallic behavior. Compared to the bare HOPG substrate, A166 was much less conductive and behaves as almost an insulator. These spectroscopic curves were taken over a wide area and using the sample heat treated asphaltene prepared multiple times on HOPG substrate by cleaving HOPG and applying the sample again. Measurements were taken in the same manner as with thin films instead of detailing architecture from on structure or sample signifying repeatability.

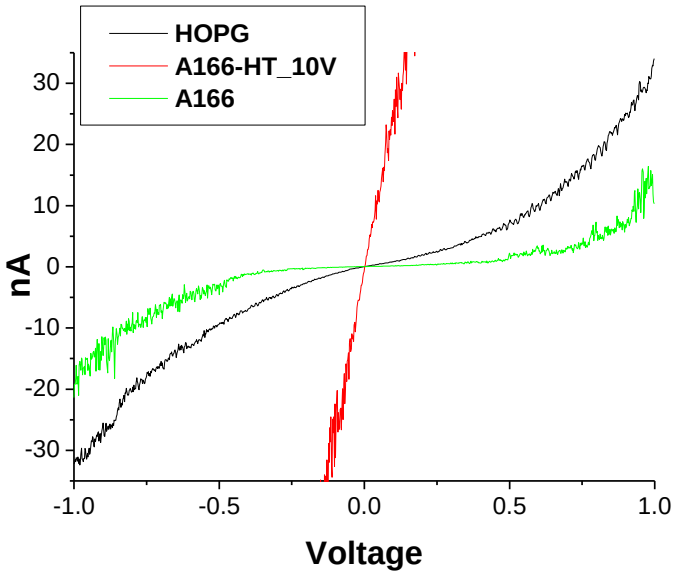

Figure 5.8. Scanning Tunneling Spectroscopy I-V spectra of bare HOPG and asphaltene covered graphite surfaces.

5.4. Conclusion

We show that heat treated asphaltene mesophase self assembles from solution into metallic nanowires due to the alignment of stacked aromatic cores. We show that heat treatment contributes to a large increase in conductivity in the sample due to the loss of insulating hydrogen groups, the increase in sp^2 hybridization and the stacking of aromatic cores. We used DFT to predict this behavior and explain the materials conductivity with increasing a continuous density of states at the Fermi energy. This material shows potential use in nanowires and molecular electronics as we were also able to use the same method to predict a conductivity greater than single layer graphene. It represents a class of carbon conductors that rivals carbon nanotubes in part because of its metallic behavior but also its low cost self-assembly.

References

[1] J. Heath, M. Ratner, Molecular Electronics, Phys. Today. (2003). http://www.nanowerk.com/nanotechnology/reports/reportpdf/report52.pdf (accessed March 24, 2017).

[2] J.S.C. Kilby, Turning Potential into Realities: The Invention of the Integrated Circuit (Nobel Lecture), ChemPhysChem. 2 (2001) 482–489. doi:10.1002/1439-7641(20010917)2:8/9<482::AID-CPHC482>3.0.CO;2-Y.

[3] R.L. Carroll, C.B. Gorman, The Genesis of Molecular Electronics, Angew. Chemie Int. Ed. 41 (2002) 4378–4400. doi:10.1002/1521-3773(20021202)41:23<4378::AID-ANIE4378>3.0.CO;2-A.

[4] G. E. Moore, Electronics 1965, 38, 114.

[5] G. E. Moore in Digest of the 1975 International Electron Devices Meeting, IEEE, New York, 1975, p. 1113.

[6] IHS report. Celebrating the 50th Anniversary of Moore's Law. 2015 https://technology.ihs.com/532195/celebrating-the-50th-anniversary-of-moores-law

[7] Igor L. Markov.Limits on fundamental limits to computation Nature 512, 147–154 (14 August 2014) doi:10.1038/nature13570

[8] Miranda, M. The threat of semiconductor variability. IEEE Spectrum http://spectrum.ieee.org/semiconductors/design/the-threat-of-semiconductor-variability (2012)

[9] Richard Feynman gave this talk entitled “There’s Plenty of Room at the Bottom” on December 29th, 1959, at the annual meeting of the American Physical Society at the California Institute of Technology

[10] K.S. Kwok, J.C. Ellenbogen, Moletronics: future electronics, Mater. Today. 5 (2002) 28–37. doi:10.1016/S1369-7021(02)05227-6.

[11] J.C. Ellenbogen, J.C. Love, Architectures for molecular electronic computers. I. Logic structures and an adder designed from molecular electronic diodes, Proc. IEEE. 88 (2000) 386–426. doi:10.1109/5.838115.

[12] L.A. Bumm, J.J. Arnold, M.T. Cygan, T.D. Dunbar, T.P. Burgin, L. Jones, D.L. Allara, J.M. Tour, P.S. Weiss, Are Single Molecular Wires Conducting?, Science (80-.). 271 (1996) 1705–1707. doi:10.1126/science.271.5256.1705.

[13] M.A. Reed, C. Zhou, C.J. Muller, T.P. Burgin, J.M. Tour, Conductance of a Molecular Junction, Science. 278 (1997) 252–254. doi:10.1126/science.278.5336.252.

[14] C. Joachim, J.K. Gimzewski, Analysis of Low-Voltage I(V) Characteristics of a Single C60 Molecule, Europhys. Lett. 30 (1995) 409–414. doi:10.1209/0295-5075/30/7/006.

[15] M. Dorogi, J. Gomez, R. Osifchin, R.P. Andres, R. Reifenberger, Room-temperature Coulomb blockade from a self-assembled molecular nanostructure, Phys. Rev. B. 52 (1995) 9071–9077. doi:10.1103/PhysRevB.52.9071.

[16] H. Dai, E.W. Wong, C.M. Lieber, Probing Electrical Transport in Nanomaterials: Conductivity of Individual Carbon Nanotubes, Science (80-.). 272 (1996) 523–526. doi:10.1126/science.272.5261.523.

[17] C. Dekker, S.J. Tans, A.R.M. Verschueren, Room-temperature transistor based on a single carbon nanotube, Nature. 393 (1998) 49–52. doi:10.1038/29954.

[18] C. Zhou, M.R. Deshpande, M.A. Reed, L. Jones Ii, J.M. Tour, Nanoscale metal/self-assembled monolayer/metal heterostructures, (n.d.). https://www.eng.yale.edu/reedlab/publications/84 nanopore APL97.pdf (accessed March 24, 2017).

[19] M.A. Reed, Molecular-Scale Electronics, (n.d.). https://www.eng.yale.edu/reedlab/publications/89 ProcIEEE99.pdf (accessed March 24, 2017).

[20] C. Joachim, J.K. Gimzewski, An electromechanical amplifier using a single molecule, Chem. Phys. Lett. 265 (1997) 353–357. doi:10.1016/S0009-2614(97)00014-6.

[21] *,† Robert M. Metzger, † Bo Chen, Ulf Höpfner, M. V. Lakshmikantham, Dominique Vuillaume, Tsuyoshi Kawai, Xiangli Wu, Hiroaki Tachibana, Terry V. Hughes, Hiromi Sakurai, Jeffrey W. Baldwin,Christina Hosch, Michael P. Cava, and Ludwig Brehmer, G.J. Ashwell§, Unimolecular Electrical Rectification in Hexadecylquinolinium Tricyanoquinodimethanide, (1997). doi:10.1021/JA971811E.

[22] Tans, S. J. et al. Nature (1998) 393, p. 49

[23] Chen, J. et al. Science (1999) 286, p. 1550

[24] C.W. Tang, Two- layer organic photovoltaic cell, Appl. Phys. Lett. 48 (1986) 183–185. doi:10.1063/1.96937.

[25] A. Tsumura, H. Koezuka, T. Ando, Macromolecular electronic device: Field- effect transistor with a polythiophene thin film, Appl. Phys. Lett. 49 (1986) 1210–1212. doi:10.1063/1.97417.

[26] J.H. Burroughes, C.A. Jones, R.H. Friend, New semiconductor device physics in polymer diodes and transistors, Nature. 335 (1988) 137–141. doi:10.1038/335137a0.

[27] S.R. Forrest, The path to ubiquitous and low-cost organic electronic appliances on plastic, Nature. 428 (2004) 911–918. doi:10.1038/nature02498.

[28] Y. Don Park, J.A. Lim, H.S. Lee, K. Cho, Interface engineering in organic transistors, Mater. Today. 10 (2007) 46–54. doi:10.1016/S1369-7021(07)70019-6.

[29] S. Sergeyev, W. Pisula, Y.H. Geerts, Discotic liquid crystals: a new generation of organic semiconductors, Chem. Soc. Rev. 36 (2007) 1902. doi:10.1039/b417320c.

[30] S. Laschat, A. Baro, N. Steinke, F. Giesselmann, C. Hägele, G. Scalia, R. Judele, E. Kapatsina, S. Sauer, A. Schreivogel, M. Tosoni, Discotic Liquid Crystals: From Tailor-Made Synthesis to Plastic Electronics, Angew. Chemie Int. Ed. 46 (2007) 4832–4887. doi:10.1002/anie.200604203.

[31] W. Pisula, M. Zorn, J.Y. Chang, K. Müllen, R. Zentel, Liquid Crystalline Ordering and Charge Transport in Semiconducting Materials, Macromol. Rapid Commun. 30 (2009) 1179–1202. doi:10.1002/marc.200900251.

[32] Jishan Wu, and Wojciech Pisula, K. Müllen, Graphenes as Potential Material for Electronics, (2007). doi:10.1021/CR068010R.

[33] Mark D. Watson, and Andreas Fechtenkötter, K. Müllen*, Big Is Beautiful−"Aromaticity" Revisited from the Viewpoint of Macromolecular and Supramolecular Benzene Chemistry, (2001). doi:10.1021/CR990322P.

[34] P.R. Wallace, The Band Theory of Graphite, Phys. Rev. 71 (1947) 622–634. doi:10.1103/PhysRev.71.622.

[35] A.K. Geim, K.S. Novoselov, The rise of graphene, Nat. Mater. 6 (2007) 183–191. doi:10.1038/nmat1849.

[36] F. Banhart*, The Formation of a Connection between Carbon Nanotubes in an Electron Beam, (2001). doi:10.1021/NL015541G.

[37] V. Derycke, R. Martel, and J. Appenzeller, P. Avouris*, Carbon Nanotube Inter- and Intramolecular Logic Gates, (2001). doi:10.1021/NL015606F.

[38] http://www.hindawi.com/journals/acisc/2013/426962/fig15/

[39] Christian Schonenberger. Bandstructure of Graphene and Carbon Nanotubes: An Exercise in Condensed Matter Physics. https://ocw.mit.edu/courses/physics/8-04-quantum-physics-i-spring-2013/study-materials/MIT8_04S13_BandGrapheneCNT.pdf

[40] http://www.nanoscience.com/files/5713/7961/7578/STM_Lab5-STM.pdf

[41] Mullins OC, Sheu EY, Hammami A and Marshall AG (eds) Asphaltenes, Heavy Oils and Petroelomics. New York City: Springer, 2007. Mullins OC and Sheu EY (eds): Structures and Dynamics of Asphaltenes. New York City: Plenum, 1998. Chilingarian GV and Yen TF: Bitumens, Asphalts, and Tar Sands. New York City: Elsevier Scientific Publishing Co., 1978.

[42] Amin A, Rid ng M, Shepler R, Smedstad E an Ratulowski J: "Subsea Development from Pore to Process," Oilfield Revi w 17, no. 1 (Spring 2005): 4–17

[43] Boussingault, M. (1837). Memoire sur la Composition des Bitumes. In Annales de Chimie et de Physique (Vol. 64, p. 141).

[44] R.R. Chianelli, M. Siadati, A. Mehta, J. Pople, L.C. Ortega, L.Y. Chiang, Self-Assembly of Asphaltene Aggregates: Synchrotron, Simulation and Chemical Modeling Techniques Applied to Problems in the Structure and Reactivity of Asphaltenes, in: Asph. Heavy Oils, Pet., Springer New York, New York, NY, 2007: pp. 375–400. doi:10.1007/0-387-68903-6_15.

[45] Binnig, G.; Rohrer, H. Hen. Phys. Acta 1982, 55, 726.

[46] G. Binnig, H. Rohrer, C. Gerber, E. Weibel, 7 × 7 Reconstruction on Si(111) Resolved in Real Space, Phys. Rev. Lett. 50 (1983) 120–123. doi:10.1103/PhysRevLett.50.120.

[47] Binnig, G.; Rohrer, H. Rev. Mod. Phys. 1987, 59, 615.L.E.C.

[48] Leemput, H. Kempe, Scanning Tunnelling Microscopy, Rep. Prog. Phys. 55 (1992) 1165–1240. ftp://ftp.ill.eu/pub/lss/Ekater/articles/rp920802.pdf (accessed March 24, 2017).

[49] https://www.ntmdt-si.com/spm-principles/view/constant-current-mode

[50] https://www.ntmdt-si.com/spm-principles/view/constant-height-mode

[51] http://nanoprobes.aist-nt.com/apps/HOPG%20info.htm

[52] https://www.ntmdt-si.com/spm-principles/view/iv-spectroscopy

[53] G.K. Benning, Atomic force microscope and method for imaging surfaces with atomic resolution, 1986. https://www.google.com/patents/US4724318 (accessed March 24, 2017).

[54] Phys. Rev. Lett. 56, 1986,930-933.

[55] N.M. Amer, G. Meyer, Atomic force microscopy, 1990. https://www.google.com/patents/US5144833 (accessed March 24, 2017).

[56] K. Geim and K. S. Novoselov. The rise of graphene. Nat. Mater., 2007, 6, 183–191. DOI:10.1038/nmat1849

[53] Li and R. B. Kaner. Materials science. Graphene-based materials. Science, 2008, 320, 1170 1171. DOI: 10.1126/science.1158180

[54] C. H. Sykes. Surface assembly: Graphene goes undercover. Nat. Chem., 2009, 1, 175–176. DOI:10.1038/nchem.224

[55] D. R. Dreyer, H.-P. Jia and C. W. Bielawski. Graphene Oxide: A Convenient Carbocatalyst for Facilitating Oxidation and Hydration Reactions. Angew. Chem., Int. Ed., 2010, 49, 6813–6816. DOI: 10.1002/ange.201002160

[56] Y. Zhu, S. Murali, W. Cai, X. Li, J. W. Suk, J. R. Potts, et. al. Graphene and Graphene Oxide: Synthesis, Properties, and Applications. Adv. Mater., 2010, 22, 3906–3924. DOI: 10.1002/adma.201001068

[57] C. N. R. Rao, A. K. Sood, K. S. Subrahmanyam and A. Govindaraj. Some Novel Attributes of Graphene. J. Phys. Chem. Lett., 2010, 1 (2), pp 572–580. DOI: 10.1021/jz9004174

[58] D. R. Dreyer, R. S. Ruoff and C. W. Bielawski, The chemistry of graphene oxide. Chem. Soc. Rev., 2010,39, 228-240 DOI: 10.1039/B917103G

[59] F. Kim, J. Luo, R. Cruz-Silva, L. J. Cote, K. Sohn and J. Huang. Self-Propagating Domino-like Reactions in Oxidized Graphite. Adv. Funct. Mater., 2010, 20, 2867–2873. DOI: 10.1002/adfm.201000736

[60] D. Wei and Y. Liu. Controllable Synthesis of Graphene and Its Applications Adv. Mater., 2010, 22, 3225–3241. DOI: 10.1002/adma.200904144

[61] K. S. Novoselov, A. K. Geim, S. V. Morozov, D. Jiang, Y. Zhang, S. V. Dubonos, et. al. Electric Field Effect in Atomically Thin Carbon Films. Science, 2004, 306, 666–669. DOI: 10.1126/science.1102896

[62] M. J. Allen, V. C. Tung and R. B. Kaner. Honeycomb Carbon: A Review of Graphene Chem. Rev., 2010, 110, 132– 145. DOI: 10.1021/cr900070d

[63] Y.-H. Lu, M. Zhou, C. Zhang and Y.-P. Feng. Metal-Embedded Graphene: A Possible Catalyst with High Activity. J. Phys. Chem. C, 2009, 113, 20156–20160. DOI: 10.1021/jp908829m

[64] D. Wei and J. Kivioja. Graphene for energy solutions and its industrialization. Nanoscale, 2013, 5, 10108- 10126. DOI: 10.1039/C3NR03312K

[65] S.M. Paek, E. Yoo and I. Honma. Enhanced Cyclic Performance and Lithium Storage Capacity of SnO2/Graphene Nanoporous Electrodes with Three-Dimensionally Delaminated Flexible Structure. Nano Lett., 2009, 9, 72–75. DOI: 10.1021/nl802484w

[66] D. Wang, D. Choi, J. Li, Z. Yang, Z. Nie, R. Kou, et. al. Self-Assembled TiO2–Graphene Hybrid Nanostructures for Enhanced Li-Ion Insertion. ACS Nano, 2009, 3,(4) 907–914. DOI: 10.1021/nn900150y

[67] D. Chen, H. Feng and J. Li, Graphene oxide: preparation, functionalization, and electrochemical applications. Chem. Rev., 2012, 112, 6027–6053. DOI: 10.1021/cr300115g

[68] R. Rozada, J. I. Paredes, M. J. López, S. Villar-Rodil, I. Cabria, J. A. Alonso, et. al. From graphene oxide to pristine graphene: revealing the inner workings of the full structural restoration. Nanoscale., 2015, 7, 2374-2390. DOI: 10.1039/C4NR05816J

[69] N. Zhao, X.N. Cheng, J. Yanga, M.X. Yang, S.H. Zheng and Y.Z. Zhou. Experimental study on the preparation, characterization and conductivity improvement of reduced graphene-oxide papers. Journal of Physics and Chemistry of Solids 2014; 75(10): 1141–1146. http://dx.doi.org/10.1016/j.jpcs.2014.05.008

[70] A. Furst, R. C. Berlo and S. Hooton. Hydrazine as a reducing agent for organic compounds (catalytic hydrazine reductions). Chem. Rev., 1965, 65, 51–68. DOI: 10.1021/cr60233a002

[71] K. Muthoosamy, R. G. Bai, I. B. Abubakar, S. M. Sudheer, H. N. Lim, H. Loh, et al. Exceedingly biocompatible and thin-layered reduced graphene oxide nanosheets using an eco-friendly mushroom extract strategy. International Journal of Nanomedicine., 2015, 10, 1505–1519. http://doi.org/10.2147/IJN.S75213

[72] C.Y. Su, Y.P. Xu, W.J. Zhang, JW Zhao, XH Tang, C.H. Tsai, et. al. Electrical and Spectroscopic Characterizations of Ultra-large Reduced Graphene Oxide Monolayers. Chem. Mater. 2009; 21(23), 5674– 5680. DOI: 10.1021/cm902182y

[73] J. Zhang, H. Yang, G. Shen, P. Cheng, J. Zhang and S. Guo. Reduction of graphene oxide via L-ascorbic acid Chem. Commun. 2010; 46(7), 1112–1114. DOI: 10.1039/B917705A

[74] D. R. Dreyer, A. Todd, C. Bielawski. Harnessing the chemistry of graphene oxide. Chem. Soc. Rev., 2014, 43, 5288-5301. DOI: 10.1039/C4CS00060A

[75] C. Botas, P. Álvarez , C. Blanco, R. Santamaría, M. Granda, P. Ares, et al. The effect of the parent graphite on the structure of graphene oxide. Carbon. 2012; 50(1): 275–282. http://dx.doi.org/10.1016/j.carbon.2011.08.045

[77]] S.Y. Pan and I.A. Aksay. Factors controlling the size of graphene oxide sheets produced via the graphite oxide route. ACS Nano. 2011; 5(5):4073–4083. DOI: 10.1021/nn200666r

[78] L. Zhang, J. Liang, Y. Huang, Y. Ma, Y. Wang and Y. Chen. Size-controlled synthesis of graphene oxide sheets on a large scale using chemical exfoliation. Carbon 2009; 47(14):3365–3368. http://dx.doi.org/10.1016/j.carbon.2009.07.045

[79] J. Zhao, S. Pei, W. Ren, L. Gao and H.M. Cheng. Efficient preparation of large-area graphene oxide sheets for transparent conductive films. ACS Nano. 2010; 4(9):5245–5252. DOI: 10.1021/nn1015506

[80] X. L. Wang, H. Bai and G.Q. Shi. Size fractionation of graphene oxide sheets by pH-assisted selective sedimentation. J. Am. Chem. Soc. 2011; 133(16):6338–634. DOI: 10.1021/ja200218y

[81] U. Khana, A. O'Neilla, H. Porwala, P. Maya, K. Nawazb and J.N. Coleman. Size selection of dispersed, exfoliated graphene flakes by controlled centrifugation. Carbon. 2012; 50(2):470–475. http://dx.doi.org/10.1016/j.carbon.2011.09.001

[82] Chen Z L, Kam F U, Goh R G S, Song J, Lim G K and L. Chua. Influence of graphite source on chemical oxidative reactivity. Chem Mater. 2013; (25) 2944-2949. DOI: 10.1021/cm304123s

[83] X. Qi, T. Zhou, S. Deng, G. Zong, X. Yao and Q. Fu. Size-specified graphene oxide sheets: ultrasonication assisted preparation and characterization. Journal of Materials Science 2014; 49(4): 1785-1793. doi:10.1007/s10853-013-7866-8

[84] G. Eda, Y.Y. Lin, C. Mattevi, H. Yamaguchi, H.A. Chen, I. S. Chen, et. al. Blue Photoluminescence from Chemically Derived Graphene Oxide. Advanced Materials 2010; 22(4): 505– 50. DOI: 10.1002/adma.200901996

[85] X. F. Zhou and Z. P. Liu. A Scalable, Solution-Phase Processing Route to Graphene Oxide and Graphene Ultra-Large Sheets. Chem. Commun. 2010; 46 (15):2611– 2613. DOI: 10.1039/B914412A

[86] S. Stankovich, D.A. Dikin, R. Piner, K. A. Kohlhaas, A. Kleinhammes, Y. Jia, et. al. Synthesis of graphene-based nanosheets via chemical reduction of exfoliated graphite oxide. Carbon. 2007; 45(7): 1558–1565. http://dx.doi.org/10.1016/j.carbon.2007.02.034

[87] D.V. Kosynkin, A.L. Higginbotham, A. Sinitskii, J.R. Lomeda, A. Dimiev, B.K. Price et al. Longitudinal unzipping of carbon nanotubes to form graphene nanoribbons Nature. 2009; 458 (7240) 872–876. doi:10.1038/nature07872

[88] I. Rodriguez-Pastor, G. Ramos-Fernandez, H. Varela-Rizo, M. Terrones and I. Martin-Gullon. Towards the understanding of the graphene oxide structure: How to control the formation of humic- and fulvic-like oxidized debris. Carbon. 2015; 84, 299-309. http://dx.doi.org/10.1016/j.carbon.2014.12.027

[89] C. Shi, L. Chen, Z. Xu, Y. Jiao, Y. Li, C. Wang, et al. Monitoring influence of chemical preparation procedure on the structure of graphene nanosheets. Physica E: Low-dimensional Systems and Nanostructures. 2012; 44 (7-8) 1420- 1424. http://dx.doi.org/10.1016/j.physe.2012.03.004

[90] D. R. Chowdhury, C. Singh and A. Paul. Role of graphite precursor and sodium nitrate in graphite oxide synthesis RSC Adv. 2014; 4, 15138-15145. DOI: 10.1039/C4RA01019A

[91] D.W. Lee, L. De Los Santos V., J.W. Seo, L.L. Felix, A. Bustamante D., J.M. Cole, C.H.W. Barnes, The Structure of Graphite Oxide: Investigation of Its Surface Chemical Groups, J. Phys. Chem. B. 114 (2010) 5723–5728. doi:10.1021/jp1002275.

[92] P. Scherrer, Bestimmung der inneren Struktur und der Größe von Kolloidteilchen mittels Röntgenstrahlen, in: Kolloidchem. Ein Lehrb., Springer Berlin Heidelberg, Berlin, Heidelberg, 1912: pp. 387–409. doi:10.1007/978-3-662-33915-2_7.

[93] L.G. Cançado, K. Takai, T. Enoki, M. Endo, Y.A. Kim, H. Mizusaki, A. Jorio, L.N. Coelho, R. Magalhães-Paniago, M.A. Pimenta, General equation for the determination of the crystallite size La of nanographite by Raman spectroscopy, Appl. Phys. Lett. 88 (2006) 163106. doi:10.1063/1.2196057.

[94] K. Haubner, J. Murawski, P. Olk, L. M. Eng, C. Ziegler, B. Adolphi et. al. The route to functional graphene oxide. ChemPhysChem. 2010; 11, 2131–2139. DOI: 10.1002/cphc.201000132

[95] M. J. Fernandez-Merino, L. Guardia, J.I. Paredes, S. Villar-Rodil, P. Solı́s-Fernandez, A. Martinez-Alonso et. al. Vitamin C Is an Ideal Substitute for Hydrazine in the Reduction of Graphene Oxide Suspensions. J. Phys. Chem. C. 2010; 114 (14) 6426-6432. DOI: 10.1021/jp100603h

[96] D. Marcano, D.V. Kosynkin, J. M. Berlin, A. Sinitskii, Z. Sun, A. Slesarev, et. al. Improved Synthesis of Graphene Oxide. ACS Nano. 2010; 4(8): 4806-4814. DOI: 10.1021/nn1006368

[97] S. Eigler, S. Grimm, M. Enzelberger-Heim, P. Muller and A. Hirsch. Graphene oxide: efficiency of reducing agents. Chem. Commun. 2013; 49(67): 7391—7393. DOI: 10.1039/C3CC43612H

[98] S. Park, J. An, I. Jung, R. D. Piner, S.J. An, X. Li, et al. Colloidal suspensions of highly reduced graphene oxide in a wide variety of organic solvents. Nano Lett. 2009; 9(4):1593–1597. DOI: 10.1021/nl803798y

[99] Z. Fan, K. Wang, T. Wei, J. Yan, L. Song and B. Shao. An environmentally friendly and efficient route for the reduction of graphene oxide by aluminum powder. Carbon 2010; 48(5):1686–1689. http://dx.doi.org/10.1016/j.carbon.2009.12.063

[100] Z. J. Fan, W. Kai, J. Yan, T. Wei, L. J. Zhi, J. Feng, et. al. Facile Synthesis of Graphene Nanosheets Via Fe Reduction of Exfoliated Graphite Oxide. ACS Nano 2010; 5(1):191–198. DOI: 10.1021/nn102339t

[101] Y. Liu, T. Li, M. Zhong, Y. Yang, Y. Wen and M. Wang. A green and ultrafast approach to the synthesis of scalable graphene nanosheets with Zn powder for electrochemical energy storage. J. Mater. Chem., 2011; 21(39):15449–15455. DOI: 10.1039/C1JM12599K

[102] Y. Wang, Z. Shi and J. Yin. Facile Synthesis of Soluble Graphene via a Green Reduction of Graphene Oxide in Tea Solution and Its Biocomposites. ACS Appl. Mater. Interfaces 2011; 3(4): 1127–1133. DOI: 10.1021/am1012613

[103] S. Thakur and N. Karak. Green reduction of graphene oxide by aqueous phytoextracts Carbon 2012; 50(14): 5331–5339. http://dx.doi.org/10.1016/j.carbon.2012.07.023

[104] B. Haghighi, M.A. Tabrizi. Green-synthesis of reduced graphene oxide nanosheets using rose water and a survey on their characteristics and applications. RSC Advances 2013; 3(32): 13365–13371. DOI: 10.1039/C3RA40856F

[105] W. Gao, L.B. Alemany, L. Ci and P.M. Ajayan. New insights into the structure and reduction of graphite oxide. Nat. Chem 2009; 1(5): 403-408. doi:10.1038/nchem.281

[106] Y. Si and E.T. Samulski. Synthesis of Water Soluble Graphene. Nano Lett. 2008; 8(6):1679–1682. DOI: 10.1021/nl080604h

[107] HJ Shin, KK Kim, A. Benayad, S.M. Yoon, H.K. Park, I.S. Jung, et. al. Efficient Reduction of Graphite Oxide by Sodium Borohydride and Its Effect on Electrical Conductance. Adv. Funct. Mater. 2009; 19(12): 1987–1992. DOI: 10.1002/adfm.200900167

[108] A. V. Krasheninnikov, R.M. Nieminen, Attractive interaction between transition-metal atom impurities and vacancies in graphene: a first-principles study, Theor. Chem. Acc. 129 (2011) 625–630. doi:10.1007/s00214-011-0910-3.

[109] D. Wei, Y. Liu, Y. Wang, H. Zhang, L. Huang, G. Yu, Synthesis of N-Doped Graphene by Chemical Vapor Deposition and Its Electrical Properties, Nano Lett. 9 (2009) 1752–1758. doi:10.1021/nl803279t.

[110] M. Wu, C. Cao, J.Z. Jiang, Light non-metallic atom (B, N, O and F)-doped graphene: a first-principles study, Nanotechnology. 21 (2010) 505202. doi:10.1088/0957-4484/21/50/505202.

[111] A. V. Krasheninnikov, P.O. Lehtinen, A.S. Foster, P. Pyykkö, R.M. Nieminen, Embedding Transition-Metal Atoms in Graphene: Structure, Bonding, and Magnetism, Phys. Rev. Lett. 102 (2009) 126807. doi:10.1103/PhysRevLett.102.126807.

[112] V. Tripkovic, M. Vanin, M. Karamad, M.E. Björketun, K.W. Jacobsen, K.S. Thygesen, J. Rossmeisl, Electrochemical CO 2 and CO Reduction on Metal-Functionalized Porphyrin-like Graphene, J. Phys. Chem. C. 117 (2013) 9187–9195. doi:10.1021/jp306172k.

[113] A. Titov, P. Zapol, P. Král, D.-J. Liu, H. Iddir, K. Baishya, L.A. Curtiss, Catalytic Fe- x N Sites in Carbon Nanotubes, J. Phys. Chem. C. 113 (2009) 21629–21634. doi:10.1021/jp810792d.

[115] S. Kattel, P. Atanassov, B. Kiefer, Stability, Electronic and Magnetic Properties of In-Plane Defects in Graphene: A First-Principles Study, J. Phys. Chem. C. 116 (2012) 8161–8166. doi:10.1021/jp2121609.

[116] W. Pisula, X. Feng, K. Müllen, Charge-Carrier Transporting Graphene-Type Molecules †, Chem. Mater. 23 (2011) 554–567. doi:10.1021/cm102252w.

[117] Murray R. Gray, Grant Assenheimer, and Lisa Boddez, W.C. McCaffrey, Melting and Fluid Behavior of Asphaltene Films at 200−500 °C, (2004). doi:10.1021/EF049923W.

[118] Akbarzadeh, K, Hammami, A, Kharrat, A, Zhang, D. Asphaltenes Problematic but Rich in Potential, Edmonton, Alberta, Canada, 2007 http://www.slb.com/news/inside_news/2008/20080404_asphaltenes.aspx (accessed March 24, 2017).

[119] S. Andersen, EFFECT OF PRECIPITATION TEMPERATURE ON THE COMPOSITION OF N-HEPTANE ASPHALTENES, Pet. Sci. Technol. 12 (1994) 51–74. doi:10.1080/08843759408916165.

[120] Altgelt, K. H. (1993). Composition and analysis of heavy petroleum fractions. CRC Press.

[121] J. T. Miller, R. B. Fisher, P. Thiyagarajan, and R. E. Winans, J.E. Hunt, Subfractionation and Characterization of Mayan Asphaltene, (1998). doi:10.1021/EF9800664.

[122] J.D.M. and, P.K. Kilpatrick, Comparison of Precipitation and Extrography in the Fractionation of Crude Oil Residua, (1997). doi:10.1021/EF9601125.

[123] G. Brons, J.M. Yu, Solvent Deasphalting Effects on Whole Cold Lake Bitumen, Energy & Fuels. 9 (1995) 641–647. doi:10.1021/ef00052a011.

[124] P.M. Spiecker, K.L. Gawrys, P.K. Kilpatrick, Aggregation and solubility behavior of asphaltenes and their subfractions., J. Colloid Interface Sci. 267 (2003) 178–93. http://www.ncbi.nlm.nih.gov/pubmed/14554184 (accessed March 24, 2017).

[125] M.E. Pena, A. Manjarréz, A. Campero, Distribution of vanadyl porphyrins in a Mexican offshore heavy crude oil, Fuel Process. Technol. 46 (1996) 171–182. doi:10.1016/0378-3820(95)00053-4.

[126] Thomas J. Kaminski, H. Scott Fogler, Nick Wolf, and Piyarat Wattana, A. Mairal†, Classification of Asphaltenes via Fractionation and the Effect of Heteroatom Content on Dissolution Kinetics, (1999). doi:10.1021/EF990111N.

[127] Xiaoli Yang, and Hassan Hamza, Jan Czarnecki, Investigation of Subfractions of Athabasca Asphaltenes and Their Role in Emulsion Stability, (2004). doi:10.1021/EF0301654.

[128] M.F. Ali, H. Perzanowski, A. Bukhari, A.A. Al-Haji, Nickel and vanadyl porphyrins in Saudi Arabian crude oils, Energy & Fuels. 7 (1993) 179–184. doi:10.1021/ef00038a003.

[129] E. Chouparova, A. Lanzirotti, H.F. and, K.W. Jones, N. Marinkovic, C. Whitson, P. Philp, Characterization of Petroleum Deposits Formed in a Producing Well by Synchrotron Radiation-Based Microanalyses, (2004). doi:10.1021/EF030108A.

[130] B. Ozturk, A. de-Luna-Bugallo, E. Panaitescu, A.N. Chiaramonti, F. Liu, A. Vargas, Atomically thin layers of B–N–C–O with tunable composition, Sci. Adv. 1 (2015) 1790–1798. doi:DOI: 10.1126/sciadv.1500094.

[131] http://m.phys.org/news/2015-08-cameras-material.html

[132] M. Chen, J. Liu, W. Zhou, J. Lin, Z. Shen, Nitrogen-doped Graphene-Supported Transition-metals Carbide Electrocatalysts for Oxygen Reduction Reaction, Sci. Rep. 5 (2015) 10389. doi:10.1038/srep10389.

[133] J. Cai, P. Ruffieux, R. Jaafar, M. Bieri, T. Braun, S. Blankenburg, M. Muoth, A.P. Seitsonen, M. Saleh, X. Feng, K. Müllen, R. Fasel, Atomically precise bottom-up fabrication of graphene nanoribbons, Nature. 466 (2010) 470–473. doi:10.1038/nature09211.

[134] K. Müllen, J.P. Rabe, Nanographenes as Active Components of Single-Molecule Electronics and How a Scanning Tunneling Microscope Puts Them To Work, Acc. Chem. Res. 41 (2008) 511–520. doi:10.1021/ar7001446.

[135] A. Narita, X.-Y. Wang, X. Feng, K. Müllen, S. Iijima, Arifin, K. Sato, H. Omachi, R. Kitaura, S. Irle, K. Suenaga, H. Shinohara, B. Menges, J. Reichert, X. Feng, H.J. Räder, F. Klappenberger, A. Rubio, K. Müllen, J. V. Barth, New advances in nanographene chemistry, Chem. Soc. Rev. 44 (2015) 6616–6643. doi:10.1039/C5CS00183H.

[136] S. Chandrasekhar, V.S.K. Balagurusamy, Discotic liquid crystals as quasi-one-dimensional electrical conductors, Proc. R. Soc. A Math. Phys. Eng. Sci. 458 (2002) 1783–1794. doi:10.1098/rspa.2001.0935.

[137] S.-C. Suen, W.-T. Whang, B.-W. Wu, Y.-F. Lai, Low-temperature fabrication of carbon nanofibers by self-assembling of polycyclic aromatic hydrocarbon molecules, Cit. Appl. Phys. Lett. Appl. Phys. Lett. 84 (2004). doi:10.1063/1.1707229.

[138] G. De Luca, A. Liscio, F. Nolde, L.M. Scolaro, V. Palermo, K. Müllen, P. Samorì, M.M. Nielsen, Y. Geerts, A.M. van de Craats, J.M. Warman, H. Zuilhof, E.J.R. Sudholter, J.A.A.W. Elemans, R.J.M. Nolte, Self-assembly of discotic molecules into mesoscopic crystals by solvent-vapour annealing, Soft Matter. 4 (2008) 2064. doi:10.1039/b807391k.

[139] J.H. Park, K.H. Kim, Y.W. Park, J.P.F. Lagerwall, G. Scalia, Ultralong Ordered Nanowires from the Concerted Self-Assembly of Discotic Liquid Crystal and Solvent Molecules, Langmuir. 31 (2015) 9432–9440. doi:10.1021/acs.langmuir.5b01332.

Vita

Eva Deemer obtained a B.S. in Chemistry from The University of Texas at El Paso with a minor in Physics in 2008 and was awarded Outstanding American Chemical Society Affiliate. In 2012, she joined the doctoral program in Materials Science and Engineering.

Dr. Deemer has received a number of awards for developing technologies while pursuing her degree. She founded a start-up company after winning $10,000 first place in a local venture challenge and went on to win the $100,000 investment prize out of all schools in University of Texas System from The University of Texas Board of Regents funded by the UT Horizon Fund. The team also won $10,000 from the UT transform fund during that time. Dr. Deemer and her co-founders were semi-finalists in venture capital competitions such as Global Venture Labs and the Big Idea Global Verizon Wireless business competition and have experience pitching for accelerators such as El Paso's Hub of Human Innovation, Technology Incubator and the Y-Combinator. Dr. Deemer received the $50,000 El Paso Innovation and Commercialization (EPIC) fund as a Principal Investigator during her studies. She spent time with Dr. David Ginger's group at The University of Washington studying SPM techniques and with Dr. Rodney Ruoff's group at University of Texas at Austin learning techniques for single-layer graphene growth. Dr. Deemer has two issued patents and is defending two additional patents. She worked for the Department of Chemistry as a teaching assistant in General Chemistry and Biochemistry and has participated judging for a student competition in El Paso Community College's Art and Science Research Symposium. Dr. Deemer worked as a research assistant on various projects sponsored by organizations such Hunt Energy Enterprises and The Office of Naval Research (ONR).

Dr. Deemer's dissertation "Methods for Producing Graphene from Petroleum By-Products" was supervised by Dr. Russell Chianelli. She has accepted a postdoctoral with Dr. Chianelli funded by ONR.

Permanent address: 5055 Ocotillo

El Paso, TX, 79932

This dissertation was typed by Eva Marie Deemer.